Dottorato di ricerca in Scienze Biomediche

CICLO XXXI

Department of Molecular Medicine, Human Physiology Unit

Coordinator: Chiar.mo Prof. Egidio D'Angelo

Functional and molecular skeletal muscle adaptations to a calcium sensitizer in transgenic mouse models of Nemaline Myopathy: a potential therapeutic strategy to augment muscle force

Doctoral dissertation by

Dott.ssa Elisa Minardi

Supervisor: Chiar.ma Prof.ssa Maria Antonietta Pellegrino

Academic Year: 2017-2018

“Phd is not a sprint, it is a marathon”

Index

Preface

Nemaline Myopathy is, although a rare genetic disease (1:50000), the most common among congenital myopathies (Romero *et al*., 2013) and no cure, excepts for symptomatic treatment such as mechanical ventilation and naso-gastric feeding, exists till now (Wallgren-Pettersson *et al*., 2011).

The main features are the muscle weakness and the presence of cytoplasmic inclusions called "nemaline bodies" or "rods" (Romero *et al*., 2013).

As no cure exists till now the main aim of this project was to test for Nemaline Myopathy a drug that got the fast track designation and orphan drug status by FDA for another muscular disease, in order to give to these patients a potential pharmacological treatment and improve the quality of their life.

Moreover, thanks to the possibility of using two different transgenic models of Nemaline Myopathy, another aim was to dissect the molecular and cellular alterations of skeletal muscle depending on the mutation.

Till now thirteen genes have been identified like causative of the disease (Moreau-Le Lan *et al*., 2018) but as the 25% of the cases and over half of cases are due to mutation in the ACTA1 gene (Romero *et al*., 2013), two mouse models, carrying mutations for this gene that encode the alpha-actin protein, $ACTA1^{D286G}$ and $ACTA1^{H40Y}$ mice, were analysed. The $ACTA1^{H40Y}$, a knock in mouse model, and the more recent mouse model, the transgene $ACTA1^{D286G}$, are responsible, in humans, of severe forms of Nemaline Myopathy.

Introduction

Skeletal muscle

Skeletal muscle is one of the most dynamic and plastic tissues of the human body and has a lot of important functions: it converts chemical energy into mechanical energy to generate force, maintain posture and make movements, and it contributes also to basal energy metabolism, serving as a reservoir of amino acids and carbohydrates.
Muscle mass depends on the balance between protein synthesis and degradation and both these processes are sensitive to factors such as disease, injury, exercise or nutritional status, among others (Frontera and Ochala, 2015).
The maintenance of a good muscle mass is important because it helps the body to fight stress and illness. Of relevance is, in fact, the role of the muscle as a storage of amino acids that can be used by the body when it is under stress condition or in a period of starvation, so when more energy is required.

Muscle structure

A layer of connective tissue called epimysium surrounds each muscle. The muscle is made up of different types of fibres arranged in bundles. Each bundle of fibres is surrounded by the perimysium connective tissue and, in turn, the single fibre is surrounded by another layer of connective tissue called endomysium. A single fibre contains a lot of myofibrils that are composed of well-organised structures of thin and thick myofilaments, the sarcomeres, which are the basic contractile units of the skeletal muscle, placed in series along the myofibrils and giving skeletal muscles a striated appearance. Sarcomeres are connected to their neighbours through the Z-discs, which run perpendicular to the filaments (Figure 1).
Proteins that concur to form the sarcomere structure can be divided into contractile proteins, myosin and actin, regulatory proteins, troponin and tropomyosin, and structural proteins, α-actinin, titin, nebulin and myomesin among others.
Important for the force production is the so-called “cross-bridge”, formed by the binding of the myosin to the actin, respectively the thick and the thin myofilaments (Greising *et al*., 2012).

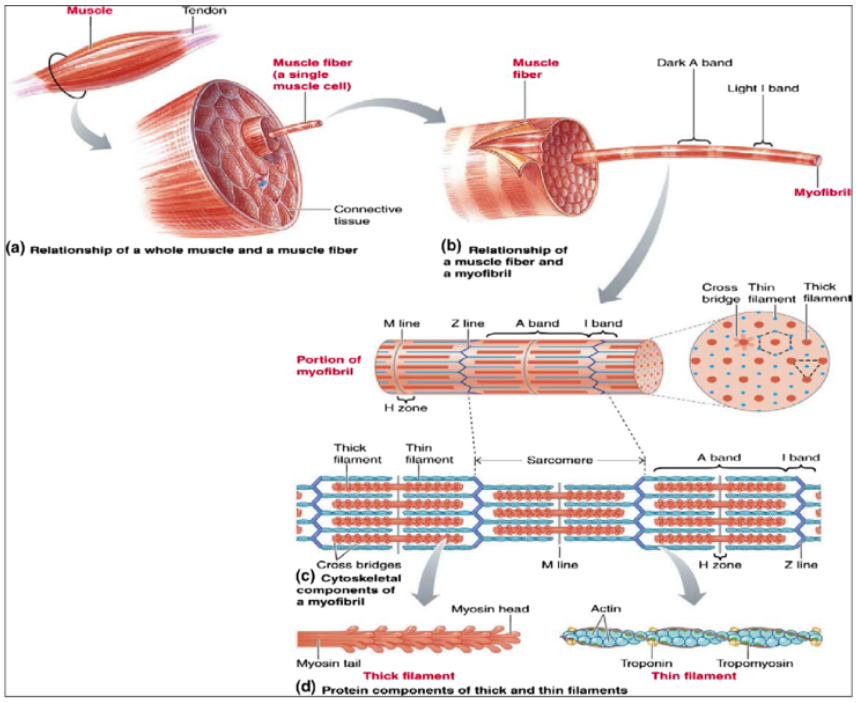

Figure 1 Skeletal muscle structure representation, from the entire muscle to the sarcomere and the contractile proteins. From Frontera and Ochala, 2015.

Fibre type diversity in mammalian skeletal muscle

Skeletal muscles were first distinguished on the basis of their colour as red or white and their contractile properties as fast or slow. The old classification, in fact, distinguished between fast-twitch muscles, characterized by glycolytic metabolism and specialized for phasic activity, generally identified with white muscles, and slow-twitch muscles, rich in myoglobin and oxidative enzymes and specialized for more continuous activity, also called red muscles.

In the last years the awareness of different fibre types evolved and physiological and biochemical studies on muscles, made up predominantly of one or another fibre type, led to the identification of four fibre types in adult mammalian skeletal muscles: type 1, 2A, 2X, 2B (Figure 2).

Moreover, immunohistochemical, biochemical and physiological studies of single fibres confirmed the existence of a spectrum of fibre types with pure or hybrid MyHC composition, according to the scheme: 1 ↔ 1/2A ↔ 2A ↔ 2A/2X ↔ 2X ↔ 2X/2B ↔

2B (Schiaffino and Reggiani, 2011).

The ability of skeletal muscles to generate force and movement is possible thanks to the nervous system. The motor tasks are postural, long-lasting and repetitive activities like respiration or locomotion and powerful actions like jumping, kicking etc. In mammals, the neuromuscular system is organized into discrete units, the motor units, each consisting of a motor neuron and all the muscle fibres it exclusively innervates. The motor units are divided on the basis of their activity as fast or slow and this is in correlation with the fibres they innervate. Motor neurons display striking differences in the firing patterns. Two classes of motor neurons, "tonic" and "phasic," have been first described 50 years ago by Granit *et al*. in 1956, and a continuous spectrum of motor neurons with distinct subgroups was later described by Henneman *et al*. in 1974.

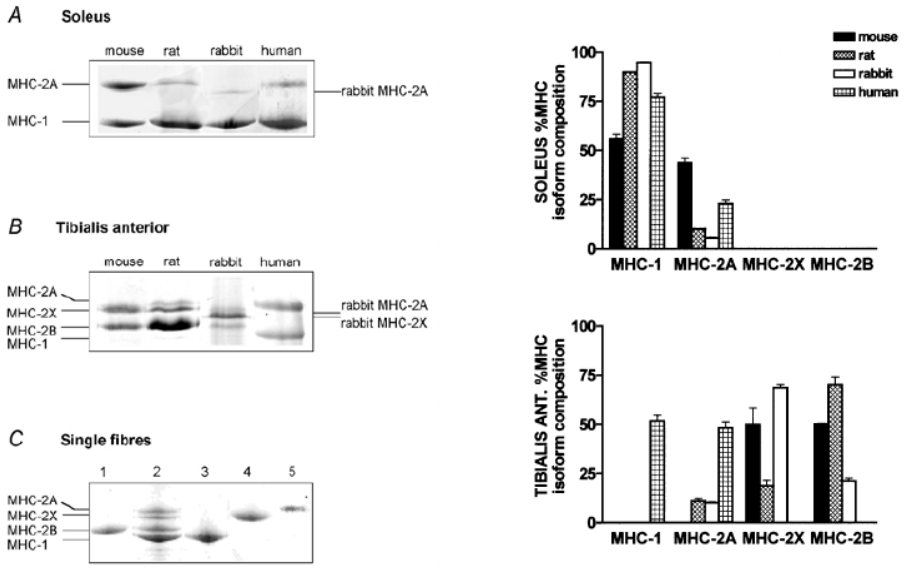

Figure 2 Mammalian myosin heavy chain (MHCs) isoforms separated by polyacrilamide gel electrophoresis (SDS-PAGE). MHC isoforms content in soleus (A), tibialis anterior (B), and single muscle fibres (C) of rat, mouse, rabbit and man. (C). From Pellegrino *et al*., 2003.

Regulation of muscle contraction: the importance of the Ca^{2+} ions

Ca^{2+} represents a powerful intracellular messenger in skeletal muscle fibres, being able not only to trigger contraction via binding to troponin, but also to activate protein phosphorylation or de-phosphorylation and proteolysis via calcium-dependent proteases.

Its intracellular concentration is regulated by the sarcoplasmic reticulum (SR), through calcium release and uptake, together with cytoplasmic calcium buffers, mitochondria and sarcolemma.

Important for the contraction is the binding of the calcium to the troponin C, a subunit of the troponin complex. In fact, troponin is made up of three interacting subunits, each of which is followed by a letter identifying its property: troponin C (TnC) binds Ca^{2+}, troponin I (TnI) binds to actin and troponin T (TnT) links the troponin complex to tropomyosin (Figure 3).

Troponin C is a two-domain protein containing in each domain calcium-binding EF motifs. The carboxy-terminal domain of troponin C (CTnC) binds calcium ions with very high affinity, stabilizing its complex with troponin I and troponin T while the N-terminal domain of troponin C (NTnC) is the regulatory domain, with one or two low-affinity calcium-binding sites. These low-affinity calcium-binding sites directly determine the calcium sensitivity of the sarcomere (Hwang and Sykes, 2015).

Troponin C is present in the myofibrils in two different isoforms, TnC-fast expressed in fast fibres that has four calcium binding sites (two high affinity and two low affinity) and TnC-cardiac-slow expressed in slow fibres that lacks one of the low-affinity sites.

The binding of the calcium to the troponin C is the first step that starts the contraction mechanism.

TnC, together with troponin T (TnT), troponin I (TnI) and tropomyosin (TM), forms a regulatory unit that controls seven actin molecules along the thin filament. In the absence of calcium, TnI and TM keep low the availability of actin binding site for myosin (blocked state). The availability of the actin molecule is increased upon binding of TnC to calcium.

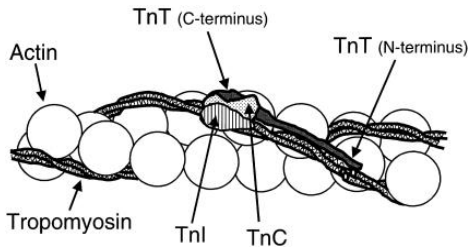

Figura 3 Troponin complex and its interaction with the tropomyosin in the actin filament. From Johnston *et al*., 2000.

Once calcium binds to troponinC, troponinI releases its inhibitory control on actin and there is a partial release of the binding of troponinT on tropomyosin to allow a tropomyosin rotational movement on the actin filament surface by about 10°. In this way, actin molecules become available to form strong hydrophobic myosin binding and this binding causes a further movement of the tropomyosin on the filament which makes all the binding sites on actin open for myosin (Schiaffino and Reggiani, 2011).

Amount of calcium that binds to troponin

The number of actin-myosin interactions during the muscle contraction depends on how many sites of actin-myosin interaction are made available during the activation process.
For each troponin C that binds the calcium, seven actin monomers are released.
The percentage of troponins that bind calcium depends on:

- The amount of calcium released by the sarcoplasmic reticulum and the amount of calcium free in the cytoplasm.
- The affinity of the troponin C for the calcium
- The time during which the calcium concentration in the cytoplasm remains at high levels before the calcium being recaptured by the sarcoplasmic reticulum.

The amount of calcium released by the sarcoplasmic reticulum after an action potential is constant as well as the affinity of the troponin C for the calcium.
The calcium released needs a certain time to reach and bind the troponin C. During this time, the calcium-pump retakes the calcium ions and tends to lower calcium concentration in the cytoplasm. After a single muscle stimulation, the cytoplasmic

calcium concentration remains high for a very short time and not all the calcium released has the time to reach the troponin C.
So, a single stimulation is not able to activate at maximal levels a muscle fibre. Repeated stimulations are needed for the maximal activation of the muscle fibre (Alloatti *et al*., 2002).

Proteins involved in the contractile mechanism

Contractile proteins

The two most abundant proteins in the muscle are actin and myosin, which form, respectively, thin and thick myofilaments within the sarcomeres and that are the main responsible of muscle force-production.

Myosin

The thick filament is primarily composed of the myosin protein (specifically myosin II), which is a hexameric protein comprising two MyHCs (~220 kDa), two essential myosin light chains ($MyLC_{17}$ - 17 kDa) and two regulatory myosin light chains ($MyLC_{20}$ – 20 kDa). The arrangement of the myosin molecule is in the way that the tail portion is positioned toward the midline of the sarcomere and the heads are directed outward to allow the binding of the myosin to the actin (Greising *et al*., 2012).

Actin

Actin is the most abundant protein in eukaryotic cells. It was isolated in 1942 by Straub as a water soluble component of muscle acetone powder (Kabsch and Vandekerckhove, 1992). The monomer is called G-actin. The G-actin crystal structure was determined in 1990 in complex with the DNasi I (Kabsch *et al*., 1990) by then more than 80 structure of actin have been discovered.

Actin exists as a monomer in low salt concentrations, but when salt concentrations, and so ionic strength, increase G-actin monomers polymerize into filaments known as F-actin.

Vertebrates present three main actin isoforms: alpha actin isoforms expressed in muscles, skeletal, smooth and cardiac muscle, beta and gamma-actin isoforms expressed in non-muscle and muscle cells, as components of the cytoskeleton and as mediators of cell motility.

Actin makes up 10 to 20% of cellular proteins and has vital roles in cell integrity, structure, and motility. It is highly conserved throughout evolution. Its function depends on the balance between monomeric (globular) G-actin (42 kD) and (filamentous) F-actin, a linear polymer of G-actin subunits.

Actin isoforms differ by only few aminoacids with the most variations in the N-terminus. Actin also undergo a lot of posttranslational modifications (Dominguez and Holmes, 2011).

Mechanism of contraction

Upon binding of ATP, myosin can dissociate from actin, breaking the acto-myosin "rigor complex," and this dissociation is quickly followed by ATP hydrolysis to P_i and ADP. Hydrolysis is accompanied by a conformational change (reverse stroke) and then followed by myosin binding to actin, in the presence of calcium ions, and subsequent release of P_i. Release of P_i is followed by a conformational change in the converter (inside the myosin head) amplified by the lever arm and transmitted to the actin filament as force or displacement (power stroke). The subsequent release of ADP leads to the formation of a new acto-myosin rigor complex, which will be in turn dissociated

by ATP binding, thus starting a new cycle (Figure 4) (Schiaffino and Reggiani, 2011).

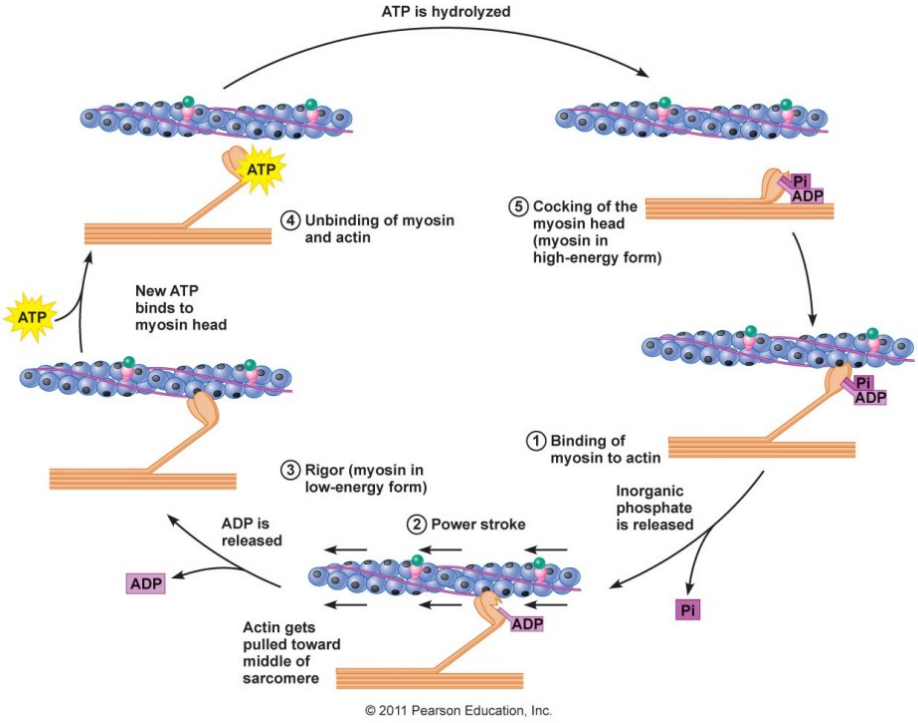

Figure 4. The different phases of the cross bridges cycle. From Stanfield. In: Fisiologia (Quarta edizione) Edises editors Cap. 12; pag 328.

ACTA1

Mutations in the ACTA1 gene represent the 25% of all the Nemaline Myopathy (NM) cases in humans and over half of the most severe forms (Romero *et al*., 2013). The majority of the patients presents with hypotonia, muscle weakness, respiratory and feeding difficulties. Moreover, the analyses of the muscle biopsies reveal the presence of cytoplasmic inclusions, the nemaline bodies, diagnostic of NM.

The ACTA1 gene encodes skeletal muscle alpha actin, the principal actin isoform in adult skeletal muscle, which forms the core of the thin filament of the sarcomere where it interacts with a variety of proteins to produce the force for muscle contraction (Laing *et al*., 2009).

Most ACTA1 mutations are missense mutations, leading the substitution of one residue in the alpha actin protein, but there can also be found nonsense mutations, splice site mutations, frameshift mutations, two amino acid duplications, mutations of the stop codon, missense mutation of two consecutive amino acid residues and insertion of an amino acid residue (Nowak *et al*., 2013). The majority of ACTA1 mutations are dominant, a small number are recessive and most isolated cases with no previous family history have de novo dominant mutations (Sparrow *et al*., 2003).

Mutations in the skeletal muscle alpha-actin gene (*ACTA1*) associated with nemaline myopathy were first described in 1999 (Nowak *et al*., 1999). These mutations were divided into two groups: (i) substitutions of residues involved in hydrophobic clusters or cores, specifically L94P, M132V, V163L and V370F; and (ii) surface-exposed residues, specifically G15R, H40Y, N115S, G182D, R183C, R256H, E259V, Q263L, N280K and D286G.

Later, a heterozygous de novo mutation in the ACTA1 gene resulting in I357L substitution, a heterozygous G268C substitution and a heterozygous I136M substitution have been identified (Ilkovski *et al*., 2001). Moreover, a novel deletion of a single nucleotide in exon 6 causing a frameshift (p. G304AfsX24) has been indicated (Friedman *et al*., 2014) as well as the de novo missense mutation N117S (Yang *et al*., 2016) and the heterozygous, missense mutation (D290H) (Ueda *et al*., 2017).

This brief excursus indicates how common, although rare, is the Nemaline Myopathy caused by ACTA1 gene.

Over the last few years, four mouse models carrying mutations in the *ACTA1 gene* and mimicking human NM have been generated (Gineste *et al*., 2013).

The first mouse model consisted of a gene invalidation, i.e. homozygous skeletal muscle α-actin knock-out mice, and mimics the human *ACTA1* recessive form of NM (Crawford *et al*., 2002). Another mouse model is a knock-in mouse model with a mutation (H40Y) in the *ACTA1* gene which causes a dominant inherited severe form of the disease in humans (Nguyen *et al*., 2011).Two mouse models carrying the D286G mutation, mimicking the mild dominant ACTA1 NM, Tg(ACTA1)(D286G), and the severe form of the disease, Tg(ACTA1)(D286G)(+/+).Acta1(+/-), have also been generated (Ravenscroft *et al.* 2011).

In this study the knock-in mouse model with the H40Y mutation and the mouse model with the D286G have been used.

ACTA1 (D286G)

The more recent mouse model expresses the *ACTA1* $^{(D286G)}$ transgene containing a mutation previously identified in a patient with a severe form of NM. This patient had no movement or respiratory effort at birth and subsequently died at 9 days of age (Agrawal *et al.*, 2004).

These Tg (ACTA1) ^{D286G} mice were less active than wild type mice and their skeletal muscles were weaker by *in vitro* analyses and showed various pathological lesions reminiscent of human patients. Their skeletal muscles contained structural abnormalities as identified in severely affected human patients, including nemaline bodies, actin accumulations and sarcomeric disarray. Furthermore, ringbinden fibres were observed in these mouse models. Nevertheless, they had a normal lifespan (Ravenscroft *et al*., 2011).

Additionally, a reduced fibre diameter indicating skeletal muscle atrophy has been reported in the version of this mouse model containing the EGFP-tag and has been associated with an on-going chronic repair and regeneration process, as illustrated by the presence of fibres with central nuclei (Ravenscroft *et al*., 2011).

Actins are a highly conserved protein family with 89% identity between cytoskeletal actin in yeast and β-actin in humans (Sheterline *et al.*, 1995) and the D286 residue is completely conserved. D286 is directly implicated in filamentous-actin subunit–subunit interactions through its involvement in the formation of a salt bridge with R39 and E270 of neighbouring actin monomers (Sheterline *et al.*, 1995) and so D286G acts as a "poison protein" (Ochala *et al*., 2012).

It was also demonstrated that this aminoacid substitution prevents proper conformational changes upon addition of Ca^{2+} and, so, less myosin-binding sites are then exposed on actin, limiting the force-generating capacity and causing muscle weakness (Figure 5) (Ochala *et al*., 2015).

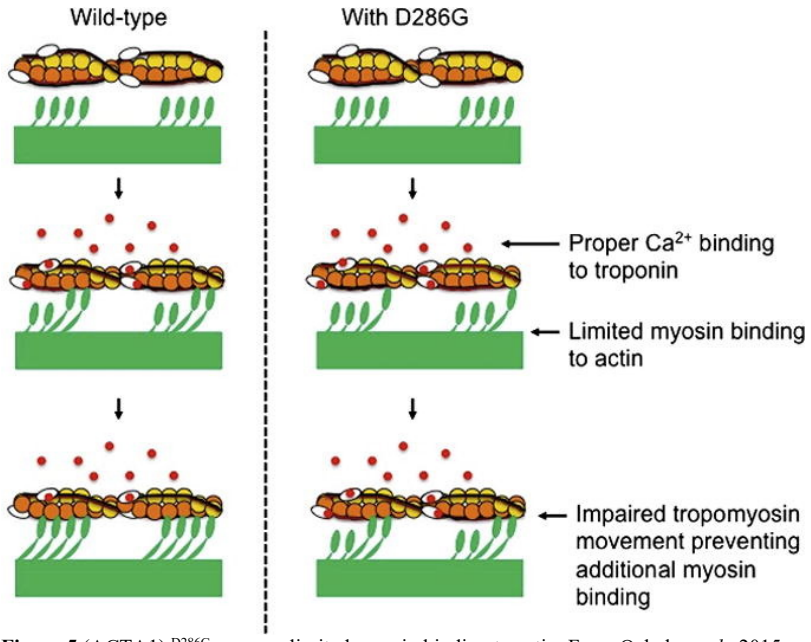

Figure 5 (ACTA1) ^{D286G} causes a limited myosin binding to actin. From Ochala *et al*., 2015.

Ravenscroft et al., moreover, found out that mice carrying this mutation showed a significant rightward shift of both pCa-force and force-frequency curves, indicating that calcium sensitivity was reduced *in vitro* in this NM model (Ravenscroft *et al*., 2011). As new pharmacological agents that increase the formation of cross-bridges at a given calcium concentration by increasing the affinity of the troponin C for calcium ions have been being tested, it could be thought that these calcium sensitizers may be useful to reduce the muscle weakness in this mouse model.

ACTA1 (H40Y)

Another NM mouse model with a mutation in the α-skeletal actin gene (Acta1) is a knock-in mouse model with the ACTA1 (H40Y) mutation (Nguyen *et al*. 2011) that causes a dominantly inherited severe form of the disease in humans (Nowak *et al*., 1999).

The Acta1 (H40Y) mouse has the features of the human condition, including early lethality, severe muscle weakness, cytoplasmic and intranuclear rods, and focal muscle repair and regeneration (Nguyen *et al*., 2011).

The shortened lifespan of the Acta1 (H40Y) mice is more severe for the male mice (52-61%) that die by 13 weeks of age, while only the 3-5% of female mice die by this time (Nguyen *et al*. 2011).

H40Y is located in actin sub-domain 2, in the DNase I-binding loop (also called D-loop, residues 38–52). The D-loop establishes an interaction with the neighbouring actin monomer by interacting with the C terminus of the adjacent subunit in actin filament. In the presence of the H40Y the actin subunits, that modulates the formation of the myosin cross-bridges and force production thanks to their extensibility, become closer, resulting in more longitudinal interactions that stiffen the filament.

Moreover, it was demonstrated with an in vitro motility assay that mutant (ACTA1 (H40Y)) and normal actin form distinct homopolimers, in fact it could be seen a Gaussian distribution for WT filaments and a biphasic distribution for filaments coming from muscles carrying H40Y mutation (Figure 6). As the H40Y reduces the number of cross-bridges and force production by 50% and the amount of mutant proteins is around 40%, it was supposed that mutant actin does not support the production of force at all (Chan *et al*., 2016).

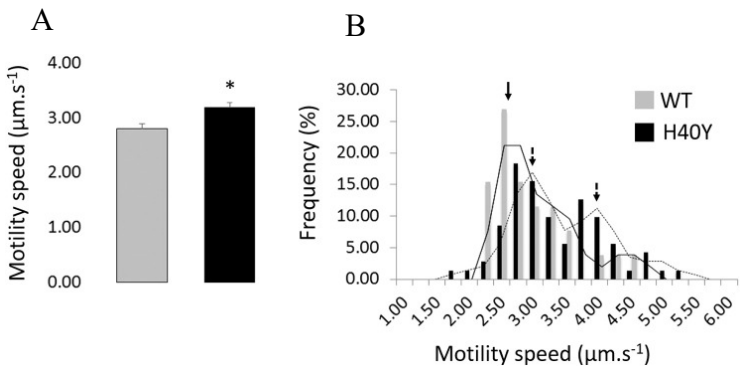

Figure 6 In vitro motility assay of filaments coming from wild type muscles and from knock in $(ACTA1)^{H40Y}$ muscles. The figure shows in the panel A the speed at which myosin molecules move WT versus H40Y actin filaments as Mean/ standard error while in the panel B it is showed the distribution of speeds for individual filaments coming from WT and H40Y mouse muscles. From Chan *et al*., 2016.

This mouse model showed also a 20% of atrophy in hindlimb muscles via MRI, confirmed by a 15-20% reduction of gastrocnemius muscle weight found *in vitro* (Gineste *et al*., 2013). Noteworthy the specific force is 25% lower in H40Y compared to controls indicating that the solely atrophy cannot explain this reduction of force, but other intrinsic muscular properties could be altered in H40Y mice. The calcium sensitivity, one parameter that could explain the higher reduction of force and that was previously found altered in both Acta1 (D286G) mouse model and patients with *NEB* or *TPM* mutations, was normal in H40Y mice, as the force-frequency curve was not altered. Finally, it was also found a higher metabolic cost in H40Y mice, as for the same energy consumption the mechanical output was lower compared to controls (Gineste *et al*., 2013).

Muscle weakness

Muscle weakness can be caused by a defect intrinsic to the muscle fibre or as a consequence of a nervous signal that does not meet the muscular fibre or is too weak to generate a muscular response. Diseases due to these problems are called myopathies that can be distinguished in primary and secondary myopathies depending if the defect is inside the muscular fibre or is due to other diseases that involve, as a consequence, the muscle. Muscle weakness is generally linked to muscle atrophy. To maintain the muscle mass is required a fine regulation and balance of two main pathways: the degradative and synthetic pathways.

Muscle atrophy can require the activation of gene transcription programs that regulate the expression of a subset of genes that are named atrophy-related genes or atrogenes involved in proteolytic pathways activation.

In addition, more than 10% of the atrophy-related genes are directly involved in energy production. Furthermore, several genes important in glycolysis and oxidative phosphorylation are suppressed in atrophying muscles, suggesting that alterations in mitochondria can have detrimental effects for the maintenance of muscle mass and function.

The decrease of muscle mass increases morbidity and impairs, moreover, the efficacy of many therapeutic treatments contributing to mortality.

Anabolic pathways

IGF/AKT/mTOR pathways

The major synthetic pathways are the IGF/AKT/mTOR pathways. Binding of the IGF1 to its receptor leads to the activation of its tyrosine kinase and its auto-phosphorylation. Moreover, the IGF1 receptor phosphorylates the insulin receptor substrate (IRS) which in turn recruits and activates the phosphatidylinositol-3-kinase (PI3K) which phosphorylates membrane phospholipids, generating phosphoinositide-3,4,5-triphosphate (PIP3) from phosphoinositide-4,5-biphosphate (PIP2). PIP3 recruits two

kinases, PDK1 and Akt, and causes the phosphorylation of Akt at threonine 308 by PDK1, leading to Akt activation (Sarbassov *et al*., 2005).

Akt inhibits protein degradation by phosphorylating, and so repressing, the transcription factors of the FoxO family and stimulates protein synthesis via the mammalian target of rapamycin (mTOR) and glycogen synthase kinase 3β (GSK3β) (Manning and Cantley, 2007).

The effect of Akt on mTOR is indirect. Akt inhibits the tuberous sclerosis complex (TSC) proteins 1 and 2 that inhibit another protein, Rheb, which causes the activation of the mTOR signalling. mTOR forms two different complexes, mTORC1 and mTORC2. mTORC2 phosphorylates Akt while mTORC1 phosphorylates the S6 kinase (S6K), which in turn phosphorylates the ribosomal protein S6 stimulating protein synthesis.

TORC1 also activates the eukaryotic translation initiation factor 4E (eIF4E) by phosphorylating the inhibitory eIF4E-binding proteins (4EBPs) (Figure 7).

The activity of the IGF1-Akt pathway is controlled by varies feedbacks. Negative feedback regulates S6K that inhibits IRS by phosphorylation, while positive feedback involves mTORC2, which phosphorylates Akt at serine 473 that, in addition to phosphorylation of Akt at threonine 308 by PDK1, causes the maximum activation of Akt (Schiaffino and Mammuccari, 2011).

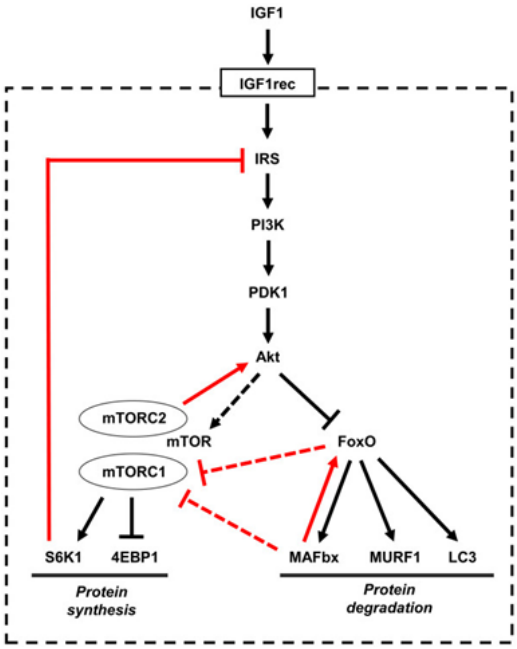

Figure 7 IGF1-Akt pathway. From Schiaffino and Mammuccari 2011.

Catabolic pathways

The degradative pathways involved in the maintenance of the muscle mass have two main components: the ubiquitin-proteasome system and the autophagy system.

THE UBIQUITIN-PROTEASOME SYSTEM

The ubiquitin-proteasome system (UPS) is the main regulatory system of protein degradation in skeletal muscle.

The UPS is an ATP-dependant process that mediates the degradation of some proteins identified by the conjugation of ubiquitin molecules.

The conjugation of the ubiquitin molecule to the target protein is mediated by the activity of three enzymes, named E1 (ubiquitin activating enzyme), E2 (ubiquitin conjugating enzyme), and E3 (ubiquitin ligase). Each E3 has specificity to its substrate, or proteins to be targeted by ubiquitination. The E3 enzyme repeat the conjugation process of the ubiquitin until a minimum of four molecules of ubiquitin are covalently

bound to the target protein and so this is recognized by the 26S proteasome as a signal to degrade the target protein.

In 2001, the mRNA levels of two skeletal muscle specific E3s, Muscle RING Finger 1 (MuRF1), and a gene designated as Muscle Atrophy F-box (MAFbx), were reported by Bodine *et al*., 2001 to be higher in all atrophied muscle models. These two E3s are called atrogenes.

The ability of the E3 protein to recognise its substrate is dependent on aminoacid sequence and/or specific structural and phosphorylated domains. MAFbx is a member of the Skp1, Cullin1 and F-box-containing proteins (SCF) complex, which bind together to establish their E3 Ub-protein ligase activity. It contains a leucine-charged residue-rich domain that binds several proteins as well as a predicted PDZ domain, cytochrome c binding site and two nuclear localisation signals, while MuRF1 contains a canonical N-terminal RING domain characteristic of RING-containing E3 ligases, followed by a MuRF family conserved region, zinc-finger domain (B-box) and leucine-rich coiled-coil domains, which allows it to form homo- and heterodimers with other MuRF proteins, and an acidic C terminal tail (Foletta *et al*., 2011).

THE AUTOPHAGY- LYSOSOME SYSTEM

Muscle cells require an efficient system for removing the unfolded and toxic proteins as well as abnormal and dysfunctional organelles. Autophagy (from Greek- "self-eating") is a process in which cytoplasmic material is degraded by the lysosome. There are three types of autophagy: (1) microautophgy, where the lysosome itself engulfs a small portion of the cytosol; (2) chaperone-mediated autophagy (CMA), in which chaperones target selective substrates to the lysosome; and (3) macroautophagy, usually termed autophagy, in which a phagophore is generated, expands, and forms an autophagosome, which can contain besides cytosol, also subcellular organelles. The autophagosome fuses with the lysosome and pours its contents into it to be degraded (Cohen-Kaplan *et al*., 2016).

There are a lot of genes that are commonly up-regulated in atrophying muscles, among these genes there some related to the autophagy-lysosome system.

Autophagosomes have been found in almost every myopathy and dystrophy studied so far and are characteristic of a group of muscle disorders named Autophagic Vacuolar Myopathies. However, it is unclear whether autophagy is detrimental and part of the mechanisms that induce muscle degeneration or whether it is a compensatory mechanism for cell survival. Some features like protein aggregation and abnormal mitochondria found in such diseases suggest an impairment of the autophagic flux (Sandri, 2010).

Several autophagy genes including LC3, Gabarap, Bnip3, VPS34, Atg12 are under FoxO3 regulation (Sandri, 2010) as well as MAFbx/atrogin-1 and MuRF1, the two atrogenes related to the ubiquitin-proteasome system (Figure 8) (Milan *et al*., 2015).

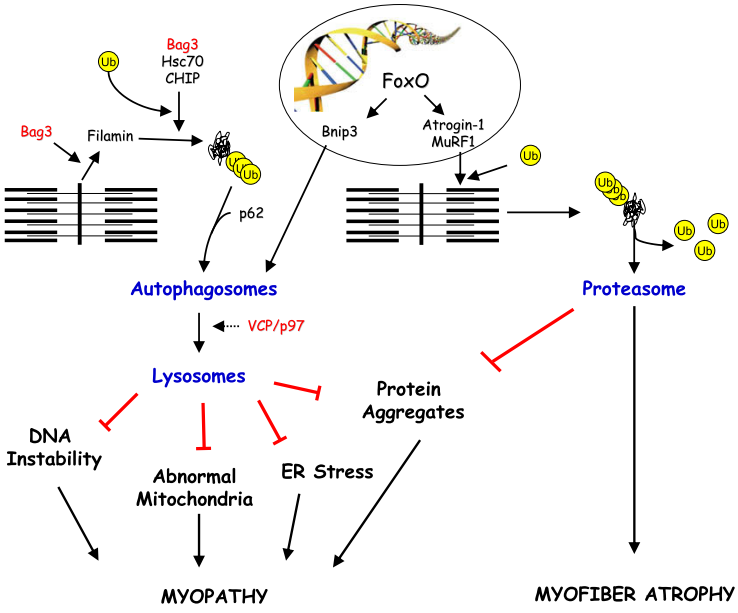

Figure 8 FoxO transcriptional activity. From Sandri, 2010.

AMPK: The energy sensor of the cell

Living cells require energy to move, grow and divide and to release molecules in the surrounding environment. This energy comes from the ATP molecules and in particular from the conversion of the ATP to ADP and phosphate. The AMPK-activated protein kinase is a ubiquitous sensor of cellular energy and nutrient status in eukaryotic cells. It monitors the AMP: ATP ratio on the basis of the reaction 2ADP <--> ATP +AMP that is maintained by all the cells close to equilibrium. If energy deficit is detected, the AMPK act to restore energy homeostasis switching on catabolic pathways and, on the contrary, switching off synthetic pathways that consume ATP.

AMPK exists in all eukaryotes as heterotrimeric complexes comprising catalytic α subunits and regulatory β and γ subunits (Figure 9). In mammals, these occur as multiple subunit isoforms (α1/α2, β1/β2, γ1/γ2/γ3) encoded by distinct genes, which can form at least 12 distinct heterotrimeric combinations. The kinase activity of the α subunit increases more than 100-fold following phosphorylation at a conserved threonine residue within the activation loop of the kinase domain (usually called Thr172) (Hardie, 2014).

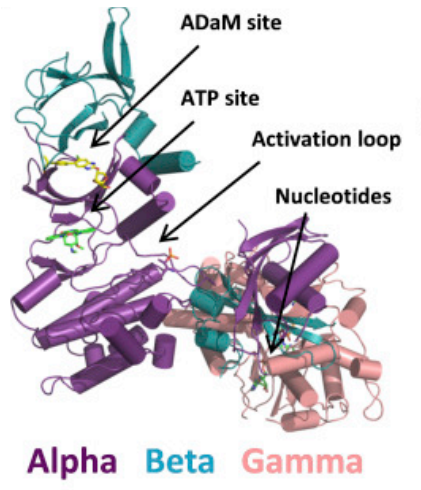

Figure 9 Structure of AMPK α1β1γ1 isoform bound to PF-739. From Cokorinos *et al*., 2017.

The major upstream kinase phosphorylating the conserved threonine residue is identified in a complex containing the tumor suppressor kinase LKB1, the pseudokinase STRAD, and the scaffold protein MO25. Then was discovered also that

Thr172 is phosphorylated by calmodulin- dependent kinase kinases (CaMKKs), especially CaMKKb (Hardie, 2014).

The downstream targets of AMPK well characterised till now are around 30 but in general phosphorylating targets are those that switch on catabolic pathway and switch off anabolic pathways. These effects are mediated by multiple mechanisms and could be both short-term and long-term effect. In fact, for example, activation of glucose uptake can occur by both translocation of GLUT4 to the membrane or by increasing the transcription of the GLUT4 gene that requires more time and has a long-term effect. However, in the longer term, AMPK activation also increases mitochondrial biogenesis by up- regulating the transcriptional co-activator PGC-1α, which in turn increases the expression of mitochondrial genes as well as the replication of mitochondrial DNA (Hardie, 2011).

PGC1alpha

PGC1alpha is a transcriptional co-activator that interacts with other transcriptional factors. It is a member of the PGC transcription co-activators family that share a high degree of homology in the N-terminus and C-terminus. The N-terminus of all of these proteins contains a transcriptional activation domain and includes the major nuclear hormone receptor-interacting motif. The C-terminal region contains an RNA-binding motif and a serine-arginine-rich domain (Puigserver and Spiegelman, 2003).
PGC1alpha is highly expressed where mitochondria are abundant and oxidative metabolism is active, including brown adipose tissue, the heart, and skeletal muscle. It is, in fact, the master regulator of mitochondrial biogenesis and is affected by muscle activity and energy stress. Its expression is also found in the brain, kidney, and at a very low level in white adipose tissue (Puigserver *et al*., 1998). PGC1a promotes also the switching of the type of fibres from glycolytic to more oxidative ones and is known to inhibit muscle atrophy by inhibiting FoxO3 (Sandri *et al*., 2006).
It was also demonstrated that overexpression of this gene prevents the activation of the catabolic pathway and, so, the disuse muscle atrophy. As a consequence, the alteration of oxidative metabolism and mitochondrial biogenesis are not the consequence of the disuse but the major cause of muscle mass wasting (Cannavino *et al*., 2014).

Mitochondria and the muscle

Mitochondria were first only known as the powerhouse of the cell because of their contribute in the production of the cellular energy by oxidative phosphorylation (OXPHOS), but now it is widely acknowledged that they are important for a lot of other processes like cell death, innate immunity, autophagy, redox signalling, calcium homeostasis and stem cells reprogramming.
They are dynamic organelles present in all eukaryotes cells that continually fuse and divide (Figure 10). The balance between these two processes regulates mitochondrial number, size and their distribution throughout the cytoplasm and is referred to as “mitochondrial dynamics”.
They have their own DNA, the mitochondrial DNA, maternally inherited, and consist

of two different membranes, the inner and the outer membranes. The space between the inner and the outer membranes is called intermembrane space. The inner membrane surrounds the mitochondrial matrix and contains respiratory complexes for oxidative phosphorylation. The outer membrane mediates the exchange between the cytosol and the intermembrane space.

The mitochondrial dynamics is under the control of the mitochondrial membrane potential (ΔΨ) across the inner membrane; dissipation of ΔΨ inhibits mitochondrial fusion while the re-establishment of ΔΨ recovers the fusion protein network (Ishihara *et al*., 2004).

They don't have a fixed shape but generally an elongated one. This is well known until their first description; in fact, mitochondrion comes from the Greek words μίτος "thread" e χόνδρος "berry", suggesting the heterogeneity of their morphology. This heterogeneous morphology is justified by their dynamic nature (Liesa *et al*., 2009).

The components of the fusion and fission machinery, involved in mitochondria dynamics and their regulation, are a lot and were identified thanks to different studies in different organisms.

Fusion machinery

The first gene involved in the fusion machinery of the mitochondrial dynamics was identified in the *Drosophila melanogaster* model (Hales and Fuller, 1997) and is called Fuzzy onions protein (Fzo).

In mammalian cells Mfn1 and Mfn2 were identified as the human homologs of the Drosophila Fuzzy onions protein.

The most important proteins involved in the mitochondrial fusion of mammals are mitofusin 1 and 2 (Mfn1 and Mfn2), located in the outer mitochondrial membrane, and OPA1 (optic atrophy-1) located in the inner membrane and intermembrane space (Liesa *et al*., 2009).

Mfn1 and Mfn2 are anchored to the mitochondrial outer membrane through the C-terminal membrane binding domain and extrude the N-terminal GTPase domain to the cytoplasm. Mfn1 and Mfn2 are widely expressed in many tissues although their

expression vary among tissues. Many experiments demonstrated that both mitofusins and their GTPase domains are essential for the fusion mitochondrial process (Ishihara *et al*., 2004).

As far as Opa1 is concerned, in humans and mice there are several splicing variants expressed in a tissue-specific manner. Some variants are cleaved in order to generate a short soluble Opa1 (Opa1S) from long Opa1 isoforms (Opa1L). It is anchored to the inner mitochondrial membrane through a transmembrane domain at the N-terminus (Romanello and Sandri, 2016).

Fission machinery

Mitochondrial fission depends on the cytosolic GTPase dynamin-related protein1 (Drp1). Drp1 is recruited in the outer mitochondrial membrane where it assembles itself into multimeric ring complexes that form active fission sites. Its recruitment on the outer mitochondrial membrane is dependent on mitochondrial membrane proteins that act as receptors. Drp1 interacts with the integral OMM proteins. In yeast Fis1 is the major DRP1 receptor. In mammals Fis1 is not the only protein to whom DRP1 are anchored in the outer mitochondrial membrane, in fact, conditional deletion of Fis1 in some experiments showed no defect in mitochondrial fission, indicating Fis1 is not essential for fission. Recently, new components of the mitochondrial fission machinery have been identified like Mff, MiD49 and MiD51 (Otera *et al*., 2010; Palmer *et al*., 2011).

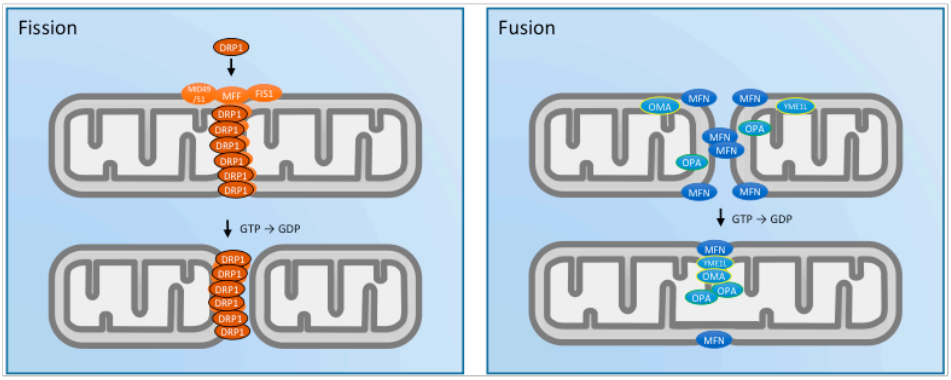

Figure 10 Mitochondrial fission and fusion and relative proteins involved. From Trewin *et al*., 2018.

Reactive species and the impact on skeletal muscle

It is widely known that contracting skeletal muscle generates reactive oxygen and nitrogen species (ROS and RNS) and that prolonged physical activity can cause oxidative damage to active myofibers. Among these, the main free radicals usually present in the cells are the superoxide ($O_2^{\bullet -}$), generated for the incomplete reduction of oxygen in the electron transport chain, and the nitric oxide (NO), generated during some enzymatic reactions. In general radicals can be formed by losing or gaining of a single electron.

Although a lot of evidences suggest that high levels of free radicals can be deleterious for the cellular components, physiological levels of radicals play important role in the cell.

ROS (Reactive Oxygen Species) is a termed used not only for oxygen centred radicals but also non-radicals that are reactive derivatives of oxygen like hydrogen peroxide (H_2O_2). At the same way, RNS refers to both nitrogen radicals and reactive species where the reactive centre is the nitrogen. ROS and RNS are commonly and collectively referred to as RONS (Reactive Oxygen and Nitrogen Species).

Among RONS we can find:

Superoxide generated by many biochemical reactions. It is negatively charged and cannot cross easily cell membranes, but protonation of superoxide forms hydroperoxyl radicals ($HO_2^{\bullet}$) that seems to cross cell membranes. Superoxide has a long half –life that gives the time to spread within the cell increasing the number of targets (Salvador

et al., 2001).

Hydrogen peroxide (H_2O_2) a non-radical ROS that is stable, has a long half-life and is permeable to cellular membranes. It is a weak oxidizing agent but at high level is cytotoxic. A lot of enzyme systems can generate the hydrogen peroxide, included the superoxide dismutases and amino acid oxidases (Halliwell and Gutteridge, 2007).

Nitric oxide (NO) synthesized in many cells from L-arginine. This synthesis occurs through three NO synthases (NOS): 1) neuronal NOS (NOS1); endothelial NOS (NOS3); and 3) inducible NOS (NOS2). Its major actions in cells are linked to its ability to bind to the ferrous ion in guanyl cyclase; this activates guanyl cyclase and promotes the formation of cyclic GMP (Halliwell, 1994). At rest, isolated skeletal muscle fibres produced low levels of NO but this production is increased during muscle contractions.

Reactive Oxygen and Nitrogen Species (RONS) and skeletal muscle force production

It is known that ROS and RNS production have an impact on skeletal muscle force production. A lot of evidences suggest that NO production shifts the force-frequency curve to the right without decreasing maximal tetanic force production.

Also ROS production has an impact on skeletal muscle force. Low levels of ROS present in skeletal muscle during resting conditions are essential for normal force production and a modest increase in ROS production results also in an increase in force production. Nevertheless, the positive impact of ROS on skeletal muscle force production is reversed as the ROS production becomes higher and higher (Reid *et al*., 1993).

In literature, in fact, is reported that qualitative adaptations, like protein post-translational modification such as phosphorylation and oxidation, could contribute to the impairment of muscle fibre structure and function more than quantitative adaptations such as the loss of myosin and other proteins (Brocca *et al*., 2017) and in an other work it was also seen that, in a condition of sarcopenia, the reduction of carbonylated proteins after an antioxidant treatment reduced also the drop of specific force even if it did not rescue muscle atrophy (Carnio *et al*., 2014).

Reactive Oxygen Species (ROS) production in mitochondria

Mitochondria are one of the main sources of ROS. In mammals, more than 95% of consumed daily oxygen is reduced to water in the respiratory chain, and 1–2% of it seems to be converted to $O_2^{\bullet -}$ by proteins in the electron transport chain in mitochondria (Culotta *et al*., 2006).

Eleven sites that produce $O_2^{\bullet -}$ an/or H_2O_2 have been identified to date in mammalian mitochondria.

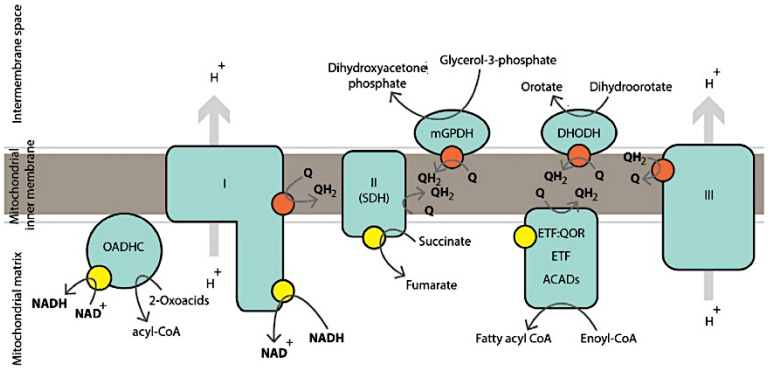

Figure 11 Mitochondrial complexes. Taken and revised from Wong *et al*., 2017.

Mitochondrial enzyme complexes oxidize a wide variety of substrates to support mitochondrial respiration (Figure 11). The rate of H_2O_2 production varies depending on the substrate mitochondria oxidize. The oxidation of the succinate leads to the highest production of $O_2^{\bullet -}$ and H_2O_2, while the rate of $O_2^{\bullet -}$/ H_2O_2 production with glutamate plus malate as substrate was considerably lower, only 20–25% of the rate with succinate, showing the importance of the source in determining the rate of mitochondrial reactive oxygen species production.

Changes in bioenergetic states by, for example, physical exercise or amount of food entrance, can influence mitochondrial substrate availability and, as a consequence, the rate of ROS production and the contribution of the different mitochondrial sites.

Generally mitochondrial complexes I and III are recognized as the major sites of mitochondrial ROS production. Exercise is associated with an increase in free radicals production and *ex vivo* findings demonstrate the heterogeneity of mitochondrial ROS

production during rest, mild and intense exercise. Also the caloric restriction can alter the ROS production. It was demonstrated that caloric restriction could decrease the ROS production of mitochondria while overnutrition could increase it (Wong *et al*., 2017).

Antioxidant defence system

Cells have a lot of protective systems, such as enzymatic and non-enzymatic antioxidants, that work together against ROS.

Superoxide dismutase was discovered in 1969 (McCord and Fridovich, 1969) and protects cells against superoxide radicals. SOD dismutates superoxide radicals to form hydrogen peroxide (H_2O_2) and oxygen (O_2):

$$2\ O_2^{\bullet -} + 2\ H^+ < -- > O_2 + H_2O_2$$

In mammals three isoforms of SOD have been discovered till now (SOD1, SOD2 and SOD3), placed in different sites of the cell. One isoform is located in the extracellular space while the other two in the cell. SOD1 is located in both the cytosol and the mitochondrial intermembrane space. SOD2 is located in the mitochondrial matrix while SOD3 in the extracellular space (Suzuki *et al*., 2000) The activity of each superoxide dismutase relies on a specific redox active metal ion that could be manganese, iron, copper or nickel ion (Culotta *et al*., 2006).
The names for the orthologs of the metal containing SODs vary among different species. In mammals, the manganese containing SOD is referred to as SOD2, SOD3 refers to extracellular Cn/Zn SOD and SOD1 intracellular Cn/Zn SOD (Pardo *et al*., 1995).
In skeletal muscle fibres the major activity of SOD is within the cytosol (65-85%) while the remaining (15-35%) is in the mitochondria. Moreover, the SOD activity is greater in the oxidative fibres (type I fibres) than in the fastest muscle fibres with low mitochondrial volume, like type IIx and IIb fibres (Powers *et al*., 1994).

Glutathione peroxidase (GPX) catalyses the reduction of H_2O_2 to water (H_2O) or

oganic hydroperoxide (ROOH) to alcohol (ROH) using reduced glutathione (GSH).

$$2GSH + H_2O_2 \rightarrow GSSG + 2H_2O$$
$$\text{or} \quad 2GSH + ROOH \rightarrow GSSG + ROH + H_2O$$

Five different glutathione peroxidases have been reported in mammals. Although the reaction catalysed by all of them is similar, they are different for substrate specificity and cellular localization (Brigelius-Flohe, 1999).
Similar to the SOD enzyme the the GPX activity is higher in oxidative fibres than in fibres with the low oxidative capacity. Moreover, the GPX activity is inducible in skeletal muscles and increase during exercise training (Powers *et al*., 1994).

GSH is the most important non-enzymatic antioxidant in muscle fibres. GSH is synthetized in the liver and then moved to tissues via the blood. The distribution of GSH varies among tissues. Tissues that have the highest concentration of oxidants have also the highest amount of GSH. So, the oxidative fibres have the higher amount of GSH than fast glycolytic fibres.
GSH can react directly with ROS by donating a hydrogen atom but can also act indirectly against ROS by serving as a substrate for GPX.
Moreover, muscle fibres adapt themselves to high intensity endurance exercise increasing the production of GSH. This increase is due to the higher activity of the enzyme that produces GSH during exercise.

Catalase is a ubiquitous antioxidant enzyme that catalyses the reduction of hydrogen peroxide (H_2O_2) into water (H_2O) and oxygen (O_2).

$$2H_2O_2 \rightarrow 2H_2O + O_2$$

Catalase requires iron as a cofactor for the reaction (Kirkman and Gaetani, 2007). Although catalase and glutathione peroxidase have common substrates, catalase has a lower affinity for H_2O_2 than GPX (Sies, 1985). Similar to both the SOD and the GPX, catalase has the higher activity in oxidative fibres than in glycolytic fibres (Powers *et al*., 1994).

Oxidative stress

The oxidative stress is defined as an alteration in the "oxidant-antioxidant balance" in favour of the first. A persistent pro-oxidant environment in cells can damage cellular structures and modify redox-sensitive molecules.

There are a lot of biomarkers that have been found in order to determine if the tissue is under a condition of oxidative stress.

Some biomarkers are the oxidants but an increase in oxidant production is not sufficient in itself to assess a pro-oxidant condition.

Other biomarkers are the antioxidants in tissues and the oxidized molecules. (Halliwell and Gutteridge, 2007). Antioxidants work against free radicals and can neutralize oxidants. Antioxidants systems consist, as it has just said, of enzymatic antioxidants such as superoxide dismutase (SOD), catalase (CAT) and glutathione peroxidase (GPxs) as well as non-enzymatic antioxidants. The enzymatic antioxidants have more effective protective effects against oxidative attack due to their ability to decompose ROS (He *et al*., 2017). Protein carbonyls are generated by the oxidation of several amino acid side chains and are measured as indicatos of protein oxidation. They are the most general and widely used biomarkers of severe protein oxidation both in vitro and in vivo, with several assays developed for their quantification. The chemical stability of protein carbonyls makes them suitable targets for laboratory measurement, in fact their stability was demonstrated even after 10 years of storage at -80°C (Dalle-Donne *et al*., 2006).

The last biomarker is the measurement of the redox balance by measure the ratio of GSH to GSSG. Increased oxidant production results in diminished GSH/GSSG ratio (Halliwell and Gutteridge, 2007).

Congenital myopathies

Congenital myopathies are a heterogeneous group of disorders, ranging in severity, characterized by the predominance of particular histopathological features on muscle biopsy. The onset of different myopathies presents the same clinical features: hypotonia, delayed motor development and muscle weakness; so, to distinguish among different myopathies, the analyses of the muscle biopsies, both with the optic and electronic microscopy, is important, and represent the first step in order to detach particular fibre abnormalities that can direct towards the correct diagnosis.
Nevertheless, some overlapping morphological abnormalities can be found and so, for assigning a definitive diagnosis, the genetic analysis is required.
A large number of genes are involved in congenital myopathies. There is, sometimes, a genetic heterogeneity within the same myopathy and, moreover, mutation in a single gene may cause diverse forms of congenital myopathies; for example, mutation in the ACTA1 gene may cause nemaline myopathy, actin filament aggregate myopathy, congenital fibre type disproportion and cap disease (Romero and Clarke, 2013).
Under these circumstances, a correct diagnosis requires the combination of different type of analyses: morphological, genetic and phenotypic analyses.

Nemaline myopathy

Nemaline Myopathy (NM), although it is a rare genetic muscular disease, is the most common among non-dystrophic congenital myopathies, with an incidence of 1:50000 live births in humans (de Winter *et al*., 2013), even if it may be more common in certain populations (e.g. in Ashkenazi Jews, or in the Amish community) (Cassandrini *et al*., 2017).
This disease was first detected in 1958 by Douglas Reye at the Royal Alexandra Hospital of Sydney in a biopsy of a 3 years old child, but this discovery was discarded until this disease was, then, described by two groups (Shy *et al*., 1963 and Conen *et al*., 1963), simultaneously, in 1963.
The diagnostic features are the muscle weakness and the presence of the so-called nemaline bodies in the sarcoplasm of the myofibres, which appear red in a green-blue myofibrillar background with the modified Gomori thrichome technique.

Nemaline Myopathy was so called from the greek word "νημα" that stands for thread, because of the nemaline bodies, that are thread-like structures (Clarkson *et al*., 2004).
To date, thirteen genes are known to be involved in this disorder, most of which encode thin filament proteins and thin filament-associated proteins: α-tropomyosin-3 and β-tropomyosin (TPM3 and TPM2), nebulin (NEB), actin α1 (ACTA1), troponin T 1(TNNT1), cofilin-2 (CFL2), LMOD3 and MYPN; other three proteins: KBTBD13, KLHL40 and KLHL41, that belong to the kelch family protein, involved in the ubiquitination and protein degradation, appear to regulate the stability and the turnover of the thin filament; finally, MYO18, is an unconventional myosin and TNNT3 encodes skeletal troponin-T_{fast} (Moreau-Le Lan *et al*., 2018).
Its inheritance can be autosomal-dominant, sporadic or autosomal recessive.
From a clinical point of view, with NM are called a heterogeneous group of myopathies, ranging in severity from a neonatal lethal disorder to a mild weakness in the adulthood (Ilkovski *et al*., 2001).
In most cases the disease progress slowly: few patients can lose the ability of walking, while, occasionally, muscle weakness can progress quickly, leading to severe respiratory problems.
Muscle weakness affects most commonly the face, neck flexors, and proximal limb; moreover, distal muscles may also be involved. Bulbar weakness and respiratory insufficiency are common, particularly in the congenital forms, and respiratory failure is the most common cause of death. Cardiac involvement is uncommon and intelligence is usually normal (North *et al*., 1997).
In 1999, the 70th European Neuromuscular Centre (ENMC) International Consortium on Nemaline Myopathy defined six clinical subtypes of nemaline myopathy, based on age of onset and the severity of clinical features (Romero *et al*. 2013). These subtypes are a severe congenital (neonatal) form, an Amish form, an intermediate congenital form, a typical congenital form, a childhood-onset form, and an adult-onset (late-onset) form (Romero *et al*., 2013).
To date, there are no effective therapies for NM, except for the symptomatic treatments, such as mechanical ventilation and nasogastric feeding.

“Nemaline bodies” or “rods”

The defining feature of all the cases of Nemaline Myopathy is the presence of bodies, within the cell, red stained with the Gomori tricome stain technique in a green-blue background. These bodies are in general rod-shaped, the why are called “rods”, but not often are visible with the optic microscope, especially if the fibres are very small like the newborn ones. For this reason the use of the electron microscope is the best technique for their analyses (Malfatti and Romero, 2016).

The rods are electron-dense inclusions with the electron microscope and their number is not correlated with the age of onset and the severity of the disease (Romero *et al*., 2013). As there is no correlation between the nemaline bodies formation and the severity of the disease (Ilkovski *et al*., 2001), Sztal et al., thanks to the creation of overexpression and loss of function zebrafish models for the ACTA1 gene, investigated on the formation of the nemaline bodies and their role in pathogenesis, discovering that they are really dynamic and transitory. They performed time-lapse experiments and showed for the first time that nemaline bodies form at the site of muscle attachment at around 30hpf and then expanded in the muscle cell. As the development went on the nemaline bodies were seen to move from the site of the muscle attachment towards the cytoplasm. So the nemaline bodies were found to be highly dynamic rather than being fixed in the Z-disk as always thought (Sztal *et al*., 2015). It was also seen that then the characteristic rod-like bodies fragmented and disappeared from the cell, coincident with the formation of the globular aggregates at the myosepta (Figure 12).

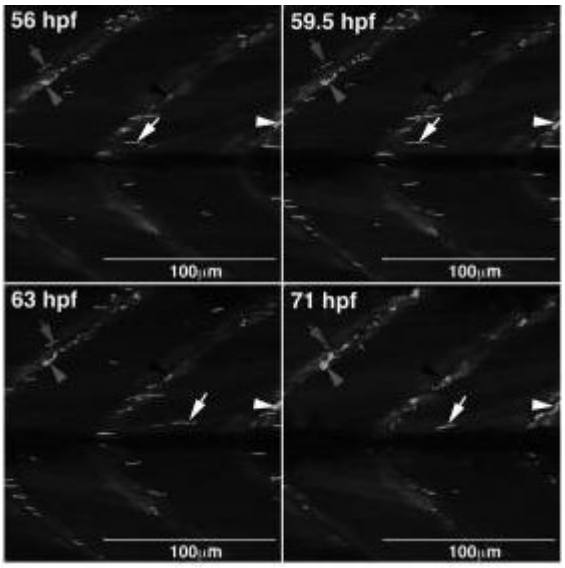

Figure 12 The arrow shows the nemaline bodie that as the development goes on it migrates from the site of muscle attachment towards the cytoplasm while disappearing. This is coincident with the formation of globular aggregates at the myosepta. From Sztal *et al*., 2015.

Moreover, the swimming behaviour after the transition from nemaline bodies into globular aggregates was impaired, suggesting that the accumulation of the actin in the cytoplasm may be detrimental for the muscle function, as they found later with a mouse model that overexpressed the ACTA1gene and that has reduced muscle performance. So, the earlier formation of globular aggregates in this model and the muscle weakness found suggested that the nemaline bodies might be part of a protective mechanism that delay the formation of the globular aggregates that are dangerous for the muscle function, as they are found also in wild type muscles under conditions of extreme stress (Sztal *et al*., 2015).

The distribution of the rods within the cell can also vary among fibres: the rods are mainly subsarcolemmal but can be found also spread within the sarcoplasm or inside the nuclei (Bruno and Minetti, 2004).

Immunohistochemical studies demonstrated they are made up of α-actinin but contain also a lot of other Z-disc proteins such as telethonin, filamin, myotilin, myozenin and myopalladin. As the main constituent of both the Z-discs and the rods is the α-actinin and the rods could appear to be in continuity with the Z-discs or like thickened Z-discs it was thought the rods to originate from Z-discs. Then it was discovered the presence

of rods also in the absence of thickened Z-discs reaching the conclusion there are different types of nemaline bodies and that only one derives from Z-disc (Sztal *et al*., 2015). As the rods are not a unique feature of Nemaline Myopathy, only the presence of both a clinical picture of congenital myopathy and the presence of rods in the muscle biopsies can confirm the diagnosis of Nemaline Myopathy (Malfatti and Romero, 2016).

Calcium sensitizers

Transition between relaxation and contraction in skeletal muscle cells is associated with an important change in the myoplasmic level of Ca^{2+} ions.

During a muscle contraction, the action potential generated at the neuromuscular junction is propagated along the sarcolemma and thanks to the T-tubule inside the muscle fibre. The action potential let the opening of the voltage sensors located in the surface of the T-tubule, the dihydropyridine receptor (DHPR), that cause the opening of the sarcoplasmic calcium ion channels, the ryanodine receptor, to whom are linked, inducing the release of calcium into the cytoplasm of the muscle fibre. Then the calcium ions bind to the troponin C and initiate a cascade of processes that brings to muscle contraction.

In patients with reduced calcium sensitivity more calcium in the cytoplasm is required to trigger contraction with a lot expense of energy. In fact, all the processes involved in the calcium handling require ATP molecules.

Calcium sensitizers are new compounds that increase muscle force augmenting the calcium sensitivity of the troponin. These are compounds that stabilizes the active form of the troponin (Pollesello *et al*., 2016)

Increasing the calcium sensitivity, the muscle, at a given calcium concentration, develop more force and this helps patients to do with less expense of energy daily activities. In this way, the energy required for the release and re-uptake of calcium should be the same as the controls.

The calcium sensitizers that have been tested till now belong to two different categories: calcium sensitizers targeting slow fibres and those targeting fast fibres.

The slow fibres calcium sensitizers are successfully used for reducing problems in cardiac disorders **(**Ochala, 2010), but now, calcium sensitizers targeting fast fibres have been being tested for other muscular disorders that not affect the hearth, as in these cases the calcium sensitizers targeting slow fibres should display many problems. These calcium sensitizers targeting fast fibres are considered the new generation of calcium sensitizers as they should be safer for the patients.

Also for the nemaline myopathy disease calcium sensitizers were used in order to find a new potential treatment for these patients. In 2013 de Winter *et al*. tested *in vitro* a troponin activator of the fast fibres that increased the muscle strength at submaximal calcium levels of muscle cells from nemaline myopathy patients with nebulin mutation (de Winter *et al*., 2013). Then, in 2015, de Winter *et al*. tested a slow troponin activator *in vitro* in order to see if these could increase the muscle force in fibres from nemaine myopathy patients with mutation always in the nebulin gene but this compound, the levosimendan, displayed no effect on force production of both the fibres of the nemaline myopathy patient with nebulin mutation and control skeletal muscle fibres (de Winter *et al*., 2015). As there are a lot of types of nemaline myopathy these calcium sensititzers should be tested for all of them in order to test their efficacy, as it is known that some mutations cause a reduced calcium sensitiveness while others not, and to give to these patients an effective potential treatment.

Aim of the work

Nemaline Myopathy, although a rare genetic disease, is the most common congenital myopathy. Patients with this disease experience muscle weakness that, if progressive, can seriously affect their daily life. Muscles main involved are the neck flexors, the diaphragm and the proximal limbs, even if, depending of the type and severity of Nemaline Myopathy, other types of muscle can be weak (Romero *et al*., 2013). Noteworthy, the weakness of the diaphragm is the primary cause of death in these patients (Ryan *et al*., 2001).

In order to improve the quality of life of these patients and help them to live and perform easily daily task, a lot of compounds have been being tested, most of which aim to restore muscle strength enhancing the capacity of the muscle to form cross-bridges at a given calcium concentration. These compounds are the so called "calcium sensitizers", most of which enhance the affinity of the troponin C for calcium and help the muscle to produce more force at a given calcium concentration.

The more recent generation of these calcium sensitizers are the one targeting only the fast muscle fibres and so are safer for the patients as they do not affect the cardiac muscle.

In this project a calcium sensitizer that got the fast track designation and orphan drug status for another muscular disease was tested in order to assess its efficacy also for the Nemaline Myopathy disease.

The aim of this project was to determine the effect of the compound on the in vivo muscle function and on muscle morphology and molecular adaptations in two mouse models affected by nemaline myopathy. In particular, the experiments aimed to investigate the effect of acute and chronic treatment of the drug at the molecular and cellular level with particular attention to the effect on fibres phenotype conversion, muscle mass and intracellular pathways involved in its maintenance, redox balance and mitochondria factors. The use of two different mouse models gave us the opportunity to establish if there is a different muscle response to the pathology depending on the mutation.

Materials and Methods

Animals

Wild type and transgenic male mice (D286G) 11-12 months old were used for the acute and chronic treatment.

Wild type and transgenic female mice (H40Y) 3 months old were used for the acute treatment, while wild type and transgenic female mice around 7 months old were used for the chronic treatment. The female mice were used as the male mice have a shorter lifespan, in fact they die by 13 weeks of age (Nguyen *et al*. 2011), due to the severity of the disease, while the female mice have a longer lifespan that let us to perform the analyses.

The reason of the starting age depended on the severity of the disease, as the H40Y mice have a severe phenotype it was decided to start at an earlier age than D286G mice.

The number of animals used per group was five.

The animals for the acute study were randomly assigned to 2 groups:

- Mice treated with placebo (Wild type and transgenic)
- Mice treated with the drug (Wild type and transgenic)

The animals for the chronic treatment were divided in two groups, which received two different type of food, food with a compound called C and food with a compound called B. The researcher didn't know if chow C or chow B was the drug or the placebo, this was a double-blind study.

The animals of all experimental groups were killed with cervical dislocation to allow removing the hindlimb muscles (EDL, tibialis anterior, gastrocnemius) and the diaphragm muscle. Muscles were weight, immediately frozen in liquid nitrogen and stored at −80 ˚C for all studies.

Animals Treatment

The acute treatment was performed as one intraperitoneal injection of the compound and then the mice were killed after 45 minutes from the injection.

The chronic treatment was performed with chow as a double-blind study.

The animals, both the wild types and the transgenic mice, were divided in two groups and one group received the chow b while the other the chow c for 4 weeks.

Morphological Investigation

Sections with a thickness of 10 μm were obtained from all the muscles using a Leica cryostat. The working temperature, to ensure the consistency suitable for the cutting of muscles, was set at -20/22°C. The sections were placed on glass slide polarized. The slides thus obtained were stained with Hematoxylin-eosin and/or anti-MHCs. The cross-sectional area of each muscle fibre was determined using the ImageJ analysis software.

Hematoxylin – eosin staining

The slides stored at -30/40°C were taken and left at room temperature for a while, then a procedure of hydration was performed.

Procedure

The slides were transferred in decreasing percentage of alcohol solutions (absolute-95%-80%-70%-50%) and then in distilled water.

Subsequently each slide was put in a solution of hematoxylin for 10 seconds and then washed with distilled water in order to remove the excess of staining.

After this step, the slide was put in a solution with eosin for 1 second and then washed again with water to remove the excess of eosin. The slides were passed through increasing percentage of alcohol solutions (50%-70%-80%-95% absolute-xylen+absolute and xylene) and after this were sealed with a cover slips fixed with Eukitt ® Mountant (Bio-Optica).

Sections so stained were analysed using a computerized image analyzer, consisting of a camera (Digital Vision) placed on a microscope (Leitz, Laborlux D) and connected through a digital interface to a computer equipped with specific software (Twain, 32).

Anti-MHCs staining

The slides stored at -30/40°C were taken and left at room temperature for a while, then were stained with mouse monoclonal antibodies specific for the different myosin heavy chain isoforms, in order to identify the different types of fibers present in each muscle. The antibodies used were as follows: BA-F8 specific for MHC-1 isoform, SC-71

specific for the MHC-2A isoform. The antibody reaction was detected subsequently by staining with peroxidase.

The primary antibodies were diluted (dilution 1:15 for BA-F8, 1:15 for SC-71) in a solution of PBS + BSA 1 % (w / v) (PBS = aqueous solution containing NaCl 136 mM, KCl 2 mM, Na_2HPO_4. 6 mM, 1 mM KH_2PO_4; BSA = bovine serum albumin).

The secondary antibody conjugated with peroxidase p0260 (DAKO) has been diluted 1:50 in PBS + 1% BSA (w / v).

Procedure

All the procedures have been performed at 37°C. The slides were left with primary antibody for 40 minutes; meanwhile it was prepared the secondary antibody. After this, 3 washes of 5 minutes with PBS were performed and the slides were left with the secondary antibody for other 40 minutes. Meanwhile the DAB (6 mg DAB + 6 ml PBS + 6 µl H2O2 to add just before the use) was prepared. Again three washes of 5 minutes with PBS were performed and, after this, the slides were covered with the DAB prepared before. The slides were left with DAB for 5 minutes and then the reaction was blocked with distilled water. After all the procedure the slides were dehydrated with an increasing percentage of alcohol solutions (40%-60%-90%- absolute- absolute+xylen-xylen) and then the slides were sealed with a cover slips fixed with Eukitt ® Mountant (Bio-Optica).

The cells positive immune-stained were visualized as brown coloured.

Proteomic analysis

Myosin heavy chains isoforms

Frozen muscles stored at -80°C were pulverized with a ceramic pestle. The exctraction of the myosin heavy chains from the pulverised muscles was done thanks to a buffer called Laemmli buffer. The Laemmli BUFFER 4X, (8% SDS, 20% 2-mercaptoehtanol, 40% glycerol,bromophenol blue traces, 0.25 M Tris HCl, pH 6.8) was previously prepared (Laemmli, 1970).

Procedure

The pulverized muscles were homogenized with Laemmli and the Eppendorf tube was frozen in liquid nitrogen. Then the tube was let defreeze at room temperature and again the two steps of freezing and de-freezing were repeated. After these steps the Eppendorf tube were left 30 minutes in ice and then centrifuged for 20 minutes at 5°C and 13500 rpm.

The Laemmli buffer was also added to the sample before the loading.

The sodium dodecyl sulfate (SDS, anionic detergent) present in the buffer has a dual function (i) being a detergent, favors the denaturation of proteins in combination with other reducing agents (beta-mercaptoethanol (ii) intercalates every two amino acids, giving the denatured protein a negative electric charge; proteins can be well resolved in accordance with their mass in an electrophoretic run. Glycerol is added to the loading buffer to increase the density of the sample to be loaded and hence maintain the sample at the bottom of the well, restricting overflow and uneven gel loading. To enable visualization of the migration of proteins it is common to include in the loading buffer a small anionic dye molecule (e.g., bromophenol blue). Since the dye is anionic and small, it will migrate the fastest of any component in the mixture to be separated and provide a migration front to monitor the separation progress. Laemmli buffer 4X was add to volume of sample that contain the total amount of proteins to load on gels at the final concentration of 1X

To visualize the MHC isoforms 12 µg of samples were loaded onto gels

To allow complete denaturation, samples are taken at 95°C for 5 minutes.

Protein concentration determination

The protein concentration of the lysates was determined using the RC DC™ (reducing agent and detergent compatible) protein assay (Bio-Rad).
RC-DC ™. is a colorimetric assay for protein determination in the presence of reducing agents and detergents. The RC DC protein assay is based on the Lowry protocol (Lowry *et al.*, 1951), one of the most used methods to evaluate protein amount; proteins in the samples are treated with copper and other solution to have a final blue coloured product which absorbance it is read at 750 nm and it is directly proportional to protein concentration according to the law of Lambert-Beer. The absorbance value of each sample is read in a spectrophotometer and the concentration protein is calculated by interpolating the values on a calibration curve whose points are scalar concentrations of a solution of known concentration (1.45 mg/ml) of Bovine serum albumin (BSA).

SDS-PAGE

The myosin heavy chain (MHC) isoform content was determined using an electrophoretic approach previously described in detail (Brocca *et al.*, 2010). Four bands could be separated in the region of MHC isoforms. Densitometric analysis of MHC bands was performed to assess the relative proportion of the four MHC isoforms, MHC-1, MHC-2A, MHC-2X and MHC-2B in each samples (Pellegrino *et al.*, 2003).
Separation and identification of myosin heavy chains (MHC) was determined by sodium dodecyl sulfate polyacrylamide gel electrophoresis (SDS-PAGE) as described by Talmadge (Talmadge *et al.*, 1996). SDS is a denaturant agent that allows proteins to separate at a migration velocity that is function of their molecular weight. SDS, indeed, binds along polypeptide chain and cancels differences in electric charge; the reduced SDS-protein complexes have the same electric charge density at a pH higher than 7. Slab gels (0.75 mm thick) were made up by a lower part, the 8% polyacrylamide running gel (composition is reported in Table A) in which took place separation of proteins; and by an upper part, the stacking gel in which wells for sample charging

were obtained. In the stacking gel, because of low concentration of acrylamide and bis-acrylamide (4%), proteins were not kept from meshes, reaching running gel uniformly. So, the migration occurred in the same way for all the bands and relative bands positions corresponded exclusively to a different molecular weight of protein.

The electrophoretic chamber was composed by an inner reservoir where was present the cathode, and by an outer one containing the anode. The two electrodes were linked to a power supply (Power Supply ESP 600) able to produce a continued current modifying voltage and amperage.

In every well 12μg of each sample were loaded. The running conditions were 200V (constant voltage) for 2 hours followed by 250V for other 24 hours. At the end of the run gel was immersed in a first solution able to fix proteins and then stained with Coomassie Blue.

In the region of MHC isoforms, four major bands were separated that corresponded, in order of migration to MHC-1 or slow, MHC-2B, MHC-2X and MHC-2A.

SOLUTION	SEPARATING GEL	STACKING GEL
ACRYLAMIDE / BIS(50:1)	8%	4%
GLYCEROL	30%	30%
SDS 10%	0.40%	0.40%
TRIS 1.5M	0.2M	
TRIS 0.5M		0.07M
EDTA		0.004M
GLYCINE	0.1M	
APS	0.10%	0.10%
TEMED	0.05%	0.05%
SOLUTION	**UPPER BUFFER**	**LOWER BUFFER**
SDS	0.10%	0.05%
TRIS	0.1M	0.5M
GLYCINE	0.15M	0.15M

Table A: 8% polyacrilamyde gel protocol

Staining with Coomassie

This method of staining can detect as little as 0.1µg of protein in a single band. After electrophoresis gel was soaked in fixing solution for 1h on a slow rotary. Then it was transferred in a small amount of Coomassie Stain. This solution dyed both protein bands and background. After a wash in water, De-staining solutions were used to remove background and maintain bands. The De-staining solution A was first used because more aggressive, the De-staining solution B was more gentle and good to keep gel for long time (table B).

SOLUTION	FIXING	COOMASSIE BLUE	DESTAIN A	DESTAIN B
METHANOL	50%	50%		
ACETIC ACID	12%	10%	10%	5%
COOMASSIE BLUE R-250		0.6%*		
ETHANOL			30%	5%

Table B: Commassie staining solutions

Densitometric analysis

The electrophoretic protocol was followed by densitometric analysis of MHC bands. It allowed the identification of isoforms and determination of the amount of an isoform respect to another one thanks to the ImageJ analysis software. During analysis protein bands were visualized as peaks and areas below peaks were measured and compared. In this way, it was possible to determine the percentage ratio between of every isoform. The analysis of each sample was repeated three times and an average of the three repeated measurements was calculated. The single value of MHC distribution obtained from each sample was averaged with the other values of subjects of the same group to assess the mean MHC isoform distribution.

Western Blot

The Western Blot technique was invented in 1979 by Towbin (Towbin *et al.*, 1979)and is a simple and rapid allows to identify a particular protein in a mixture of proteins, using the recognition by specific antibodies. The mixture of proteins (protein lysate) is first separated according to their molecular weight by electrophoresis on a polyacrylamide gel and subsequently transferred on a nitrocellulose or Polyvinylidene Fluoride (PVDF) membrane. After it is possible to proceed to the recognition of target protein through the use of a specific antibody; the binding protein-antibody can be displayed using different techniques, including coloured products or chemiluminescence autoradiography.

Samples preparation

Frozen muscles stored at -80°C were pulverized with a ceramic pestle. The powder thus obtained was homogenized with a lysis buffer containing 20mM TRIS-HCl, 1% triton x100, 10%Glycerol, 150mM NaCl, 5 mM EDTA, 100mM NaF and 2mM NaPPi supplemented with 1X inhibitors protease phosphatase (Protease Inhibitor Cocktail, Sigma-Aldrich, St. Louis MO) and 1mM PMSF. The lysis of tissue was performed on

ice for 40 minutes. The homogenate obtained was centrifuged at 13500 rpm for 20 minutes at 4°C and the supernatant was transferred to a clean eppendorf tube and stored at -80°C until ready to use. The protein concentration of the lysates was determined using the RC DC™ (reducing agent and detergent compatible) protein assay (Bio-Rad) as described above.

Electrophoresis

Gradient precast gels purchase from BIORAD (anykd) were used; in these gels the percentage of two polymers varies uniformly from 12% (the upper part of the gel) to 20% (at the bottom of the same); and they are designed to provide a complete and well resolved molecular weight protein separation pattern (300kD-5kD) The total amount of protein that was load onto gels depend on the expression level of target protein that we studied. To allow complete denaturation, samples are taken at 95°C for 5 minutes.
Equal amounts of protein sample (see table C) were loaded on the gel and subjected to electrophoresis; electrophoretic run was carried out at constant current (100V) for about 2 hours in a running buffer at pH 8.8 (Tris 25mM, Glycine 192mM, 1% SDS). To monitor proteins separation a protein molecular weight marker, constituted by a mixture of proteins with known molecular weight (Preistained Protein Ladder Marker, BIORAD), were loaded on the gel. At the end of the gel run the electrophoretic apparatus was disassembled and the gel recovered for the next step.

Electroblotting

In order to make the proteins accessible to antibody detection, they are transferred from within the gel onto a membrane made of *nitrocellulose or polyvinylidene difluoride (PVDF*). The primary method for transferring the proteins is called electroblotting and uses an electric current to extract proteins from the gel into the PVDF or nitrocellulose membrane. The proteins move from within the gel onto the membrane maintaining their organization by applying an electric field in which the proteins still negatively charged migrate from the negative (gel) to the positive pole (membrane). As a result of

"blotting" process, the proteins are exposed on a thin surface layer for detection (see below). Protein binding is based upon hydrophobic interactions, as well as charged interactions between the membrane and protein.

In this study the proteins resolved by electrophoresis, are transferred (blotting) to a PVDF or nitrocellulose membrane (for poly-ubiquitinated proteins and oxyblot). The transfer was carried out at constant voltage at 100V for 120 minutes at 4°C or 35mA overnight (O/N) in a transfer buffer containing 25mM Tris, Glycine 192mm, and 20% methanol.

The effective proteins transfer to PVDF/nitrocellulose was verified by staining with Ponceau Red (Sigma) in acetic acid (0.2% Ponceau Red in 3% acetic acid) for 5 minutes under stirring at room temperature; for polyubiquitinated proteins and oxyblot experiments ponceau stained membrane were scanned and images were used for next analysis.

Target protein detection

To minimize the background, nonspecific binding sites present on the nitrocellulose/PVDF membrane are saturated with a blocking solution consisting of 5% fat-free milk in TBST (Tris 0.02M, NaCl 0.05M and 0.1% Tween-20) or 3% BSA depending on the protein studied (Table C) for two hours at room temperature with constant shaking. At the end incubation the membrane was washed with TBST for three times 10 minutes each and incubated overnight at 4°C with the specific primary antibody appropriately diluted in a solution of TBST containing 5% BSA or 5% MILK (Table C). Subsequently, the membrane was washed three time in TBST and then incubated for 60 minutes at room temperature in constant agitation, with a secondary antibody diluited suitably goat anti-mouse or anti rabbit conjugated with the enzyme HRP (Horseradish Peroxidase) After removing the excess of antibody with two washes of 10 minutes each, in TBST and the last one in TBS (Tris 0.02M and NaCl 0.05M).
Proteins detection was made using ECL advance detection system (Amersham) which highlights the HPRT substrate with a chemiluminescent reaction.

	lysate (µg)	Block solution	Ab I	company	Ab II	company
p-AKT	30	5%MILK 2h RT	1:1000 4%BSA O/N	Cell signaling	Anti-Rabbit (1:10000) 5% MILK	Cell signaling
AKT	30	5% MILK 2 h RT	1:1000 4%BSA O/N	Cell signaling	Anti-Rabbit (1:10000) 5% MILK	Cell signaling
p-S6Rp	30	5% MILK 2 h RT	1:1000 4%BSA O/N	Cell signaling	Anti-Rabbit (1:10000) 5% MILK	Cell signaling
S6Rp	30	5% MILK 2 h RT	1:1000 4%BSA O/N	Cell signaling	Anti-Rabbit (1:10000) 5% MILK	Cell signaling
p-4EBP1	30	5% MILK 2 h RT	1:1000 4%BSA O/N	Cell signaling	Anti-Rabbit (1:10000) 5% MILK	Cell signaling
4EBP1	30	5% MILK 2 h RT	1:1000 4%BSA O/N	Cell signaling	Anti-Rabbit (1:10000) 5% MILK	Cell signaling
PGC1α	30	5% MILK	1:1000 5%MILK	abcam	Anti-Rabbit (1:10000) 5% MILK	Cell signaling

	lysate (µg)	Block solution	Ab I	company	Ab II	company
SOD1	20	5%MILK 2h RT	1:1000 5%MILK O/N	abcam	Anti-rabbit (1:10000) 5% MILK	Cell signaling
catalase	20	5% MILK 2 h RT	1:1000 5%MILK O/N	abcam	Anti-Rabbit (1:10000) 5% MILK	Cell signaling
GAPDH	30	5%MILK 2h RT	1:2000 5%MILK O/N	abcam	Anti-rabbit (1:15000) 5% MILK	Cell signaling
α-tubulin	30	5% MILK 2 h RT	1:1000 5%MILK O/N	Sigma	Anti-mouse (1:10000) 5% MILK	DAKO
Polyubiquitinated proteins	15	2%BSA 2h RT	1:5000 2%BSA 1h	Enzo life science	Anti-mouse (1:15000) 5% MILK	DAKO

Table C: antibodies list used

Analysis of data

The proteins were quantified.

The data were expressed as an integrated density (units of optical density per volume of the band). The target protein levels were then normalized to a housekeeping, the alpha-tubulin or the GAPDH. The data are expressed as the ratio between the target protein and the housekeeping

Oxyblot

Oxidative modification of proteins by oxygen free radicals and other reactive species such as hydroxynonenal occurs in physiologic and pathologic processes. As a consequence of the modification, carbonyl groups are introduced into protein side chains by a site-specific mechanism.

The protein carbonylation level was detected using the OxyBlot™ Kit (AbNova) that provides reagents for sensitive immunodetection of these carbonyl groups.

The carbonyl groups in the protein side chains are derivatized to 2,4-dinitrophenylhydrazone (DNP hydrazone) by reaction with 2,4-dinitrophenylhydrazine (DNPH). The DNP-derivatized protein samples are separated by polyacrylamide gel electrophoresis (Anykd Biorad gels) followed by Western blotting. This step is followed by blocking of nonspecific binding sites with 3% BSA solution. Then the membranes are incubated with primary antibody, specific to the DNP moiety of the proteins and subsequently with a horseradish peroxidase-antibody conjugate directed against the primary antibody (secondary antibody: goat anti-rabbit IgG). The membranes are then treated with chemiluminescent reagents (ECL advance as describe previously). The positive bands emitting light were detected by the instrument.

The oxidative status between control and unloaded mice were analyzed quantitatively by comparison of the signal intensity of immune-positive proteins normalized on total proteins amount loaded on gels (ponceau staining signal).

Myosin/actin ratio analysis

Frozen muscles stored at -80°C were pulverized with a ceramic pestle. The powder thus obtained suspended in lysis buffer (50 mM Tris-HCl pH 7.6, 250 mM NaCl, 5 mM EDTA, 1.5% v/v β-mercaptoethanol and 2% inhibitor-proteases cocktail from Sigma-Aldrich, St Louis, MO, USA). A protein assay kit (RC DC, Bio-Rad, Hercules, CA, USA) was used to determine protein concentration. For each subject 10 μg of sample were loaded into a pre- cast gradient gel (Bio Rad). The gel was run for 1 hour at room temperature at 100 V and then stained with Coomassie Blue and acquired with

a high-resolution scanner (Epson expression 1680 Pro). The BAP of myosin and actin bands of each sample was measured using the software Adobe Photoshop CS3 and the myosin/actin ratio was then calculated.

Functional analysis

Mice were anesthetised in an induction chamber with 4% isoflurane (Forene; Abbott France, Rungis, France) mixed in 33% O_2 (0.5 L/min) and 66 % N_2O (1 L/min). Once the right lower hindlimb was shaved, electrode cream was applied at the knee and heel levels in order to optimise electrical stimulation. Each anesthetised mouse was placed supine in a home-built cradle which has been specially designed to investigate gastrocnemius muscles of mice. Muscle contractions were achieved by transcutaneous electrical stimulation using two rod-shaped 1.5 mm-diameter surface electrodes integrated in the cradle and connected to an electrical stimulator (Digitimer DS7, Hertfordshire, UK).

One electrode was placed at the heel level and the other one was located just above the knee joint.

Transcutaneous stimulation was elicited with square-wave pulses (0.5 ms duration) on the gastrocnemius muscle. The individual maximal stimulation intensity was determined by progressively increasing the stimulus intensity until there was no further increase in the peak twitch force.

Gene expression analysis

RNA extraction

The muscle tissues still frozen, were pulverized using a sterile pestle and mortar previously treated with RNase Zap to remove RNAse presence. Approximately 20 mg of powder of each sample was used to RNA extraction with SV Total RNA Isolation System (Promega, Italia).

The successful isolation of intact RNA requires four essential steps: (i) effective disruption of cells or tissue, (ii) denaturation of nucleoprotein complexes, (iii) inactivation of endogenous ribonuclease (RNase) activity and (iv) removal of contaminating DNA and proteins. The most important step is the immediate inactivation of endogenous RNases that are released from membrane-bound organelles upon cell disruption. The SV Total RNA Isolation System combines the disruptive and protective properties of guanidine thiocyanate (GTC) and β-mercaptoethanol to inactivate the ribonucleases present in cell extracts. GTC, in association with SDS, acts to disrupt nucleoprotein complexes, allowing the RNA to be released into solution and isolated free of protein.

Dilution of cell extracts in the presence of high concentrations of GTC causes selective precipitation of cellular proteins to occur, while the RNA remains in solution. After centrifugation to clear the lysate of precipitated proteins and cellular debris, the RNA is selectively precipitated with ethanol and bound to the silica surface of the glass fibers found in the Spin Basket. By effectively clearing the lysate of precipitated proteins and cellular debris, these cleared lysates may be bound to the Spin Baskets by a centrifugation filtration method. The binding reaction occurs rapidly due to the disruption of water molecules by the chaotropic salts, thus favoring adsorption of nucleic acids to the silica.

RNase-Free DNase I is applied directly to the silica membrane to digest contaminating genomic DNA. The bound total RNA is further purified from contaminating salts, proteins and cellular impurities by simple washing steps. Finally, the total RNA is eluted from the membrane by the addition of Nuclease-Free Water. This procedure

yields an essentially pure fraction of total RNA after only a single round of purification without organic extractions or precipitations.

RNA quantification

Nucleic acids absorb ultraviolet light in a specific pattern. In a spectrophotometer, a sample is exposed to ultraviolet light at 260 nm, and a photo-detector measures the light that passes through the sample. The more light absorbed by the sample, the higher the nucleic acid concentration in the sample.
Using the Beer Lambert Law the amount of light absorbed was related to the concentration of RNA in samples.
We evaluated also RNA from proteins contaminants by checking the ratio of the absorbance at 260 and 280nm ($A_{260/280}$) that for pure RNA $A_{260/280}$ is ~2.

cDNA Synthesis

In order to measure messenger RNA (mRNA), it is necessary using a Reverse transcriptase enzyme to convert mRNA into complementary DNA (cDNA) which will be then amplified by Real-Time PCR .
In this study 400 ng of RNA for each sample were reverse transcribed using the Superscript III enzyme (Invitrogen) with this protocol:
At 400 ng of RNA of each sample were addicted 1µl of random primers, 1µl Deoxyribonucleosides (10mM each dATP, dGTP, dCTP and dTTP at neutral pH),and RNAse free water to reach the final volume of 13.5 µl. The mix obtained was heat at 65°C for 5 minutes and incubate on ice for at least 1 minute.
Then 4 µl of 5X First-Strand Buffer, 1 µl of 0.1 M DTT, 1 µl of RNaseOUT™ Recombinant RNase Inhibitor (40 units/µl) and 0.5 µl of SuperScript™ III RT (200 units/µl) were addicted. The mix was incubated at 25°C for 5 minutes, at 50°C for 60 minutes. Increase the reaction temperature to 70°C for 15 minutes to inactivate reaction.

Primer efficiency validation

In principle, amplicons double at each cycle. The actual production, however, depends of the efficacy of each amplification cycle.
The traditional method for determining amplification efficiency requires a calibration curve, where a sample is serially diluted at known concentration.
For each primer, a calibration curves with serial diluition (10^{-1}) was performed; Ct values obtained were blotted versus the initial amounts of input material on a semi-log10 plot, and the data were fit to a straight line. It is possible to determine the efficiency for each reaction, by calculating the slopes of the standard curves generated by using the equations:

Exponential Amplification: $10^{(-1/slope)}$ or, Reaction Efficiency:$[10^{(-1/slope)}]-1$

Optimal values for slope and efficiency are -3.322 and 1, respectively. These calculations are usually automatically determined by the software and provided with the results. In this project only primers that have an efficiency higher that 0.9 were accepted (Table D).
Specificity of each reaction as well as primers dimers possibly formation should be ascertained after completion of the amplification protocol. by performing the Melting procedure (58-99°C; 1°C/5 seconds). When most of the fluorescent signal originates from the product of interest during the amplification procedure, a single melting peak is obtained. In contrast, should there be amplification of secondary products, of primer dimers or of non-specific amplicons, several melting peaks are generated at temperatures lower than the melting point expected for the product of interest, precluding any quantitative assessment. In this study all primers pairs that showed a good efficiency but an atypical melting curve were not used for real time experiment.

GENE	FORWARD PRIMER	REVERSE PRIMER
MURF1	ACCTGCTGGTGGAAAACATC	CTTCGTGTTCCTTGCACATC
ATROGIN-1	GCAAACACTGCCACATTCTCTC	CTTGAGGGGAAAGTGAGACG
PGC-1α	ACCCCAGAGTCACCAAATGA	CGAAGCCTTGAAAGGGTTATC
FIS1	AAGTATGTGCGAGGGCTGT	TGCCTACCAGTCCATCTTTC
DRP1	GTTCCACGCCAACAGAATAC	CCTAACCCCCTGAATGAAGT
GAPDH	CACCATCTTCCAGGAGCGAG	CCTTCTCCATGGTGGTGAAGAC
MFN1, MFN2, OPA1 TaqMan gene expression assay (Applied Biosystems)		

Table D: list of primers used for gene expression experiments

Real time PCR

Real Time PCR allows reaction to be characterized by the point in time during cycling when amplification of a PCR products achieves a fixed level of fluorescence, rather than the amount of PCR product accumulated after a fixed number of cycle (PCR end-point)

An amplification plot graphically displays the fluorescence detected over the number of cycles that were performed.

As shown in Figure 13, the initial cycle of PCR, there is no significant change in fluorescence signal. This predefined range of PCR cycles is called baseline.

The software generates a baseline subtracted amplification plot by calculating a mathematical trend using Rn values (the fluorescence emission intensity of the reporter dye) corresponding to the baseline cycles. Then an algorithm search for the point on the amplification plot at which the delta Rn (Rn-baseline) crosses the treashold. The fractional cycle at which this occurs is defined as the Ct.

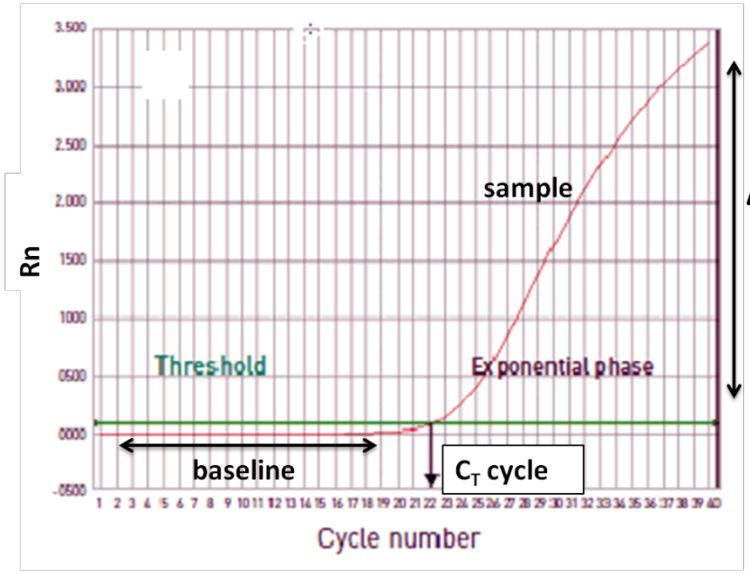

Figure 13 Reference curve of a single sample amplification plot; in the baseline no significant change in fluorescence signal (Rn) occurs, in the exponential phase fluorescence signal increase in proportional to amplification products increase formation. The threshold line is the level of fluorescence signal automatically determined by the sequence detection system software and it is set to be above the baseline and sufficiently low to be within the exponential growth region of the amplification curve. The Ct cycle is the number of amplification Cycle when the fluorescence signal cross the threshold.

Real-time PCR experiments were performed using AB 7500 instrument (Applied Byosistems); and PCR reactions were performed using SYBR Green chemistry (Power Syber Green, Applied Byosistems) and Go-Taq (Promega Corporation).

Real time PCR reaction was composed when using Syber Green by:

- 3µl cDNA
- 12µl sterile water
- 15µl Power Syber Green

and when using Go-Taq:

- 1 µl cDNA
- 12,5 µl sterile water
- 15 µl Go-Taq (2x)
- 1,5 µl Taqman primers

Each sample was run in duplicate. PCR thermal cycler parameters were set to standard mode of 10 minutes incubation at 95°C before repeat cycling at 95°C for 15 seconds, followed by a 1minute incubation at 60°C for 40 cycles; were fluorescence signal was detected. For the Taqman primers the PCR thermal cycler parameters were set as 2 minutes at 95°C, 15 seconds repeated 40 times at 95°C and 1minute at 60°C.
In all the PCR reaction was added the dissociation stage.
Differentially expressed genes were determined using a default threshold of 0.6. The difference between Ct (cycle threshold) values was calculated for each mRNA by taking the mean Ct of duplicate reactions and subtracting the mean Ct of duplicate reactions for the reference RNA, measured on an aliquot from the same RT reaction (ΔCt = Ct target gene – Ct reference gene). All samples were then normalized to the ΔCt value of a calibrator sample to obtain a ΔΔCt value (ΔCttarget – ΔCtcalibrator) (comparative method).

Statistical analyses

All the analyses were conducted using the One-Way ANOVA and, when required, the t-test. Values are mean ± standard deviation (SD) and the p value was set at <0.05.

Results and Discussion

Acute treatment

In *vivo* functional determination

The first part of this study was to test the *in vivo* effect of the acute administration of the drug (a calcium sensitizer), one injection, on force production in transgenic mice. Our partner Dr. J. Gondin and his team have done the *in vivo* muscle force experiments. The acute administration did not produce any significative improvement in *in vivo* force production, neither in the wild type nor in the transgenic mice Tg (ACTA1) ^{D286G} and Tg (ACTA1) ^{H40Y} (graph not shown).

Cellular morphology

Tg (ACTA1) ^{D286G} As one of the main features of Nemaline Myopathy is the muscle weakness and as atrophic fibres has been reported by Ravenscroft *et al*. in mice carrying the D286G mutation (Ravenscroft *et al.,* 2011), the cross sectional area of both wild type and transgenic muscles from male mice 12 months old subjected to acute treatment (one injection of the compound) was analysed. The following skeletal muscles have been analyzed: EDL, gastrocnemius, tibialis anterior and diaphragm.
Cross sectional area of single muscle fibres was determined on cross muscle cryosections obtained from the midbelly region. The mean values of CSA of Tg (ACTA1)^{D286G} muscles are presented in Figure14.

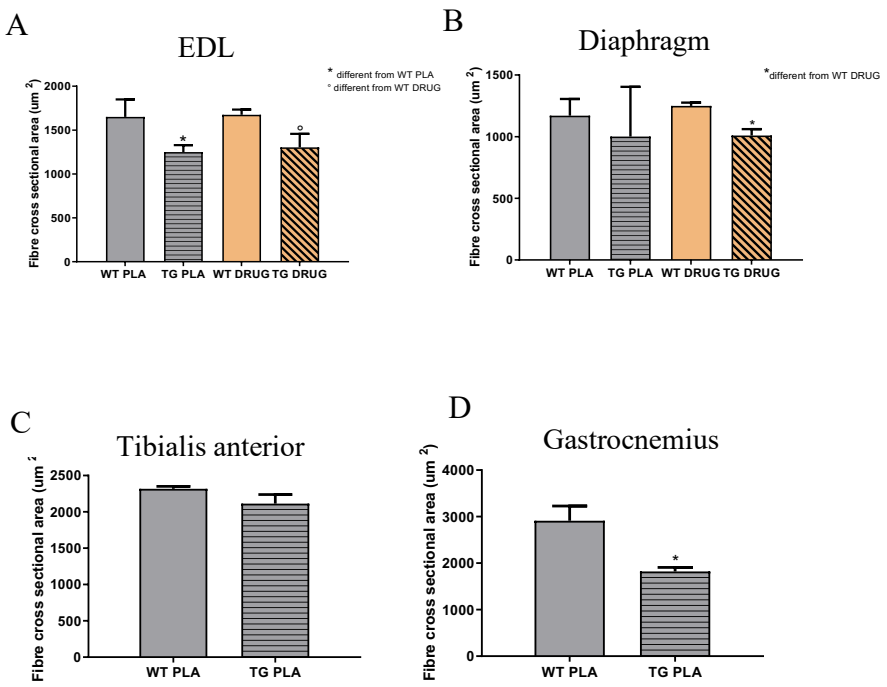

Figure 14 The graphs show the mean value of single muscle fibres cross sectional area of the EDL (A), diaphragm (B), tibialis anterior (C) and gastrocnemius (D) muscles from wild type and Tg(ACTA1)^{D286G} mice injected both with the placebo (PLA) and the drug.The data are represented as Mean values ± SD. The symbols in the figures "*" and "°" indicate a statistically significant difference (p value <0.05).

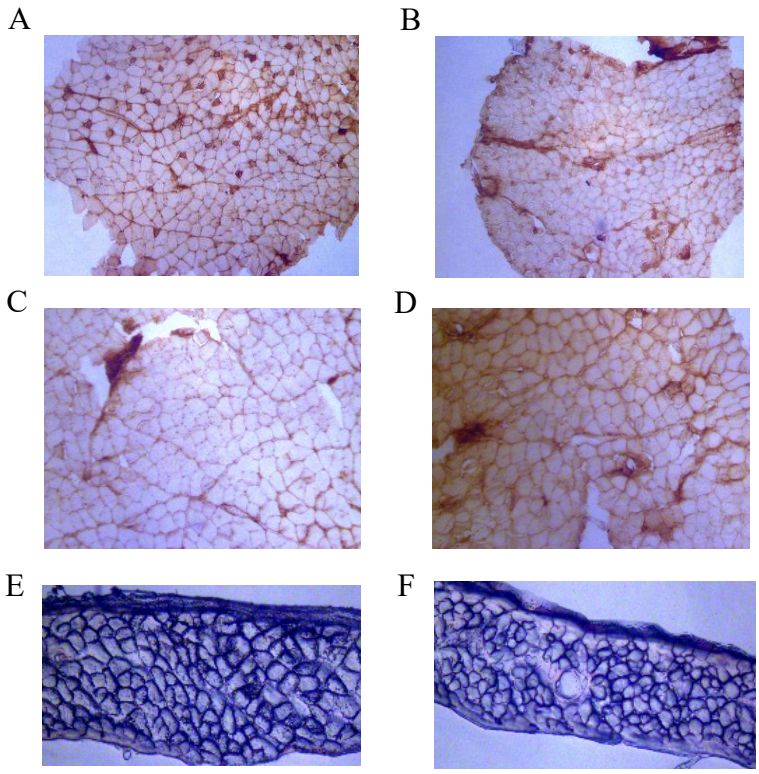

Figure 15 Images of transverse section (10μm thick) stained with antibody against MHC-2A isoform of EDL received the placebo from wild type muscle (A) and from Tg ACTA1^{D286G} muscle (B); of tibialis anterior received the placebo from wild type muscle (C) and from Tg ACTA1^{D286G} muscle (D); and , finally, of diaphragm received the placebo from wild type muscle (E) and from Tg ACTA1^{D286G} muscle (F). Acquisition of the images were done with a 10X objective.

Transgenic mice showed a significant decrease in the size of single skeletal muscle fibres of EDL, diaphragm (Figure 15) and gastrocnemius muscles, in comparison to the wild type muscles, even if for the diaphragm muscle the decrease in fibres size reaches the statistical significance only for transgenic mice fed with the drug (Figure 14). No changes in muscle size were found in tibialis anterior muscle between wild type and transgenic mice (Figure 15) suggesting that the tibialis anterior muscle is spared from the effect of the mutation (at least at this age, i.e. 12 months).

Moreover, results obtained in EDL and Diaphragm muscles indicated no effect of the compound on the muscle fibres size (Figure 14).

Tg (ACTA1)^{H40Y} The cross-sectional area results of tibialis anterior, diaphragm and gastrocnemius single muscle fibres are presented in Figure 16. No changes were found in fibres CSA of Tibialis anterior muscle and for 2A fast fibres of Diaphragm muscle among the experimental groups (Figure 17). A significant hypertrophy of slow fibres, type 1, was found in diaphragm muscle of transgenic mice respect to the wild type (Figure 16). As in D286G model, gastrocnemius muscle of transgenic mice showed a significant atrophy. Moreover, results obtained in diaphragm and tibialis anterior muscles indicated no effect of the compound on the muscle fibres size (Figure 16).

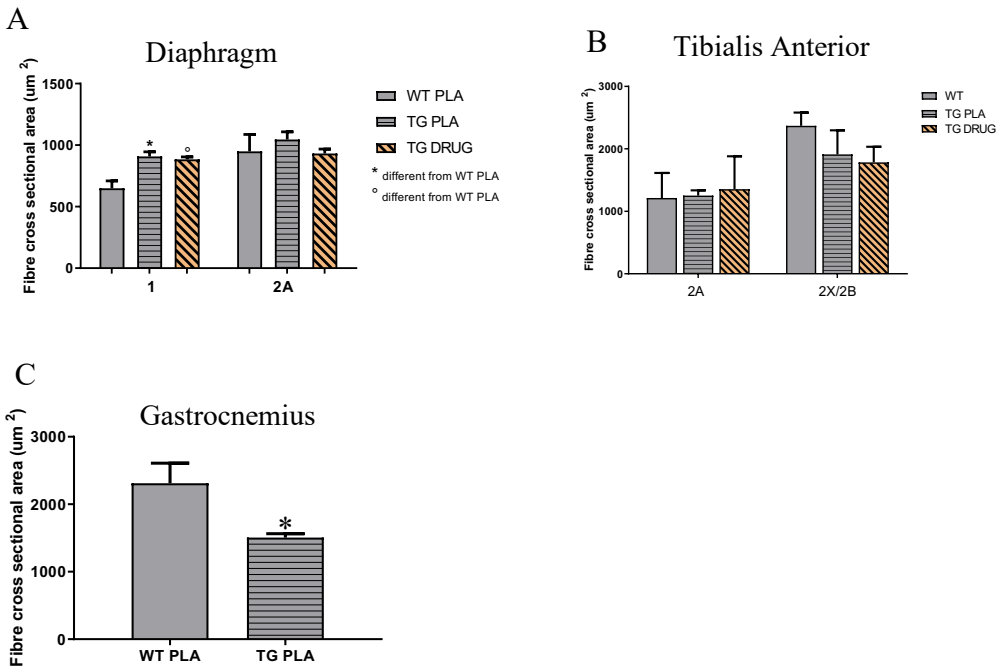

Figure 16 The graphs show mean value of fibre cross sectional area of diaphragm (A), tibialis anterior (B) and gastrocnemius (C) muscles of wild type and Tg ACTA1^{H40Y} mice injected both with the drug and the placebo (PLA). The data are represented as Mean ±SD. The symbols in the figures "*" and "°" indicate a statically significant difference (p value <0.05).

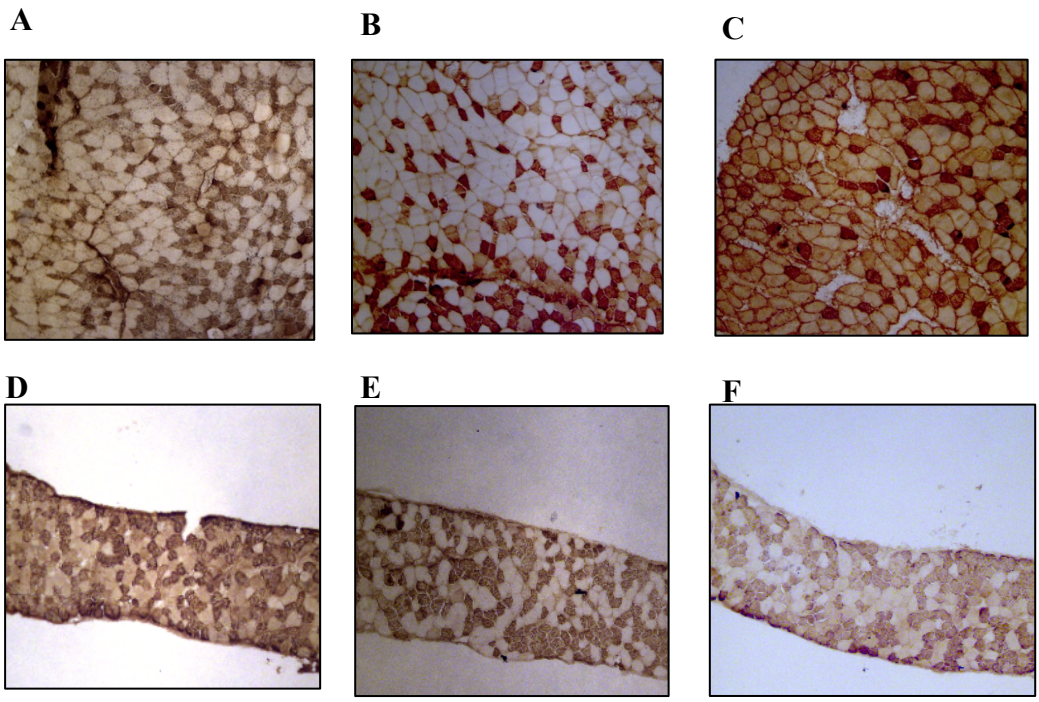

Figure 17 Images of transverse sections (10μm thick) stained with antibody against MHC-2A isoform of tibialis anterior from wild type muscle received the placebo (A), Tg ACTA1^{H40Y} muscle received the placebo (B) and Tg ACTA1^{H40Y} muscle received the drug (C) and images of transverse sections of diaphragm from wild type muscle received the placebo(D), Tg ACTA1^{H40Y} muscle received the placebo (E) and Tg ACTA1^{H40Y} muscle received the drug (F). Acquisition of the images were done with a 10X objective.

These results suggest a different adaptation of the different muscles to the pathology in the same transgenic model and also between different models.

This is in line to what was found in another nemaline myopathy mutation (the nebulin model) in which it was discovered that different muscles respond differently to nemaline myopathy. In fact it was found out a difference in trophicity among muscles, measured through the muscle weights, that varies also with the age. In this nebulin model of nemaline myopathy the gastrocnemius and quadriceps muscle weights were found 60-70% smaller than those of control muscles at all ages, while the tibialis cranialis and EDL muscles weights were smaller than those of control at 5 months of age but less at 6 months and, finally, the diaphragm and soleus muscles showed

minimal weight changes excepts at 6 months when the soleus muscle weight was increased up to 50%. (Li *et al*., 2015).

Interestingly, gastrocnemius and tibialis anterior muscles showed a common CSA adaptation in the Tg $(ACTA1)^{D286G}$ and the Tg $(ACTA1)^{H40Y}$ models, with gastrocnemius muscle significantly atrophic and tibialis anterior muscle spared from atrophy. The gastrocnemius muscle atrophy found here is in agreement with the significant reduced body weight and volume of the hindlimb muscles of transgenic mice carrying H40Y (Gineste *et al*., in 2013).

Unlike the gastrocnemius and tibialis anterior muscles, the diaphragm muscle showed a different adaptation in the two transgenic models, with muscle atrophy in the Tg $(ACTA1)^{D286G}$ model and no changes or hypertrophy in the Tg $(ACTA1)^{H40Y}$ model. Diaphragm muscle hypertrophy in the presence of the H40Y mutation has also been documented in Lindqvist *et al*. in 2013, where a compensatory mechanism has been hypothesized. Our results are in line with the idea that muscles with a higher composition of oxidative fibres, like the diaphragm muscle, do not have smaller weights and can have hypertrophy, offsetting their force deficit. In fact, it was supposed that muscles rich in type I and IIa fibres (like the diaphragm muscle) might escape the atrophic fate thanks to their baseline activity. This was supposed not only for the diaphragm but also for the soleus. In fact, as it is known, the diaphragm muscle is cyclically activated while the soleus muscle is an antigravitary muscle (Li *et al*., 2015).

Collectively, results of CSA obtained in the Tg $(ACTA1)^{D286G}$ and Tg $(ACTA1)^{H40Y}$ mice indicate a different muscles response to the nemaline myopathy disease.

Pathways involved in muscle mass maintenance

In view of the CSA results that showed a variable involvement of the different muscles in the pathology, the adaptations of the main systems that control skeletal muscle mass maintenance, i.e. the ubiquitine proteasome and the IGF-Akt pathway, were analysed with Real-time PCR and Western Blot technique.

Degradation pathway-Ubiquitin proteasome pathway

Tg (ACTA1)^{D286G} The adaptation of the ubiquitin proteasome pathway was studied through the analysis of the expression levels of two important atrogenes: MuRF1 (muscle-specific ring finger protein-1) and atrogin-1.

Figure 18 shows the mRNA level of MuRF1 and atrogin-1 in Tibialis anterior, Diaphragm and Gastrocnemius muscles. A significant down-regulation of these ubiquitin ligases was observed in all transgenic muscles in comparison with the wild type muscles, both after the placebo and the drug. The drug had no effect on these markers in all the analyzed muscles.

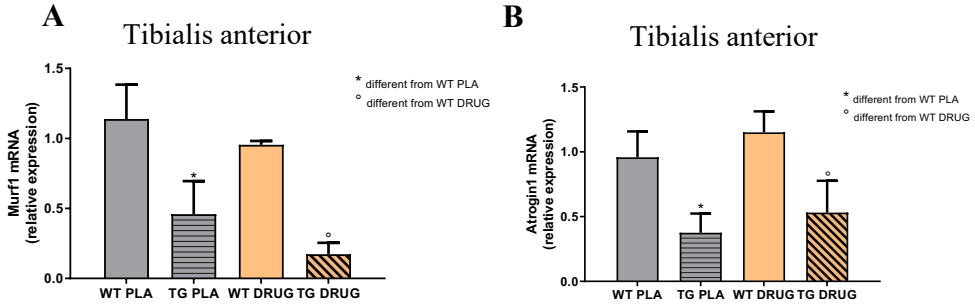

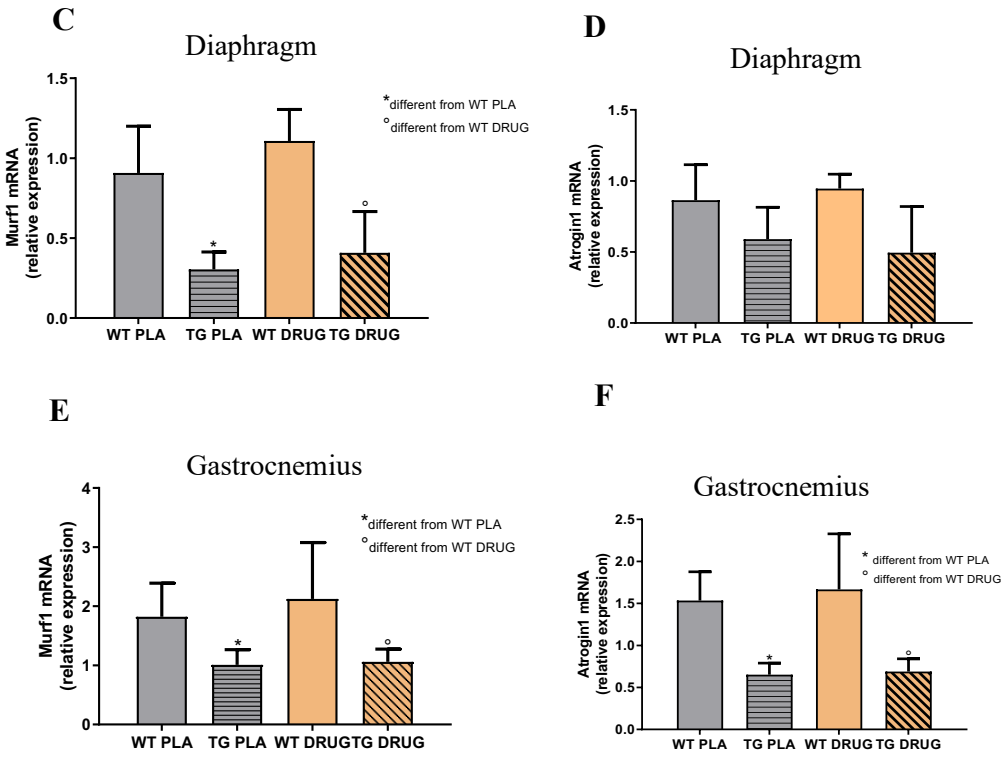

Figure 18 Relative expression of Murf1 and Atrogin1 ubiquitin ligases from wild type and Tg (ACTA1)^{D286G} muscles determined by Real time PCR. The data were normalised using the GAPDH expression. The data are represented as Mean ± SD. The symbols in the figures "*" and "°" indicate a statically significant difference (p value <0.05).

Tg (ACTA1)^{H40Y} The mRNA level of MuRF1 and atrogin1 in muscles from Tg ACTA1^{H40Y} mice are reported in Figure 19. Tibialis anterior and gastrocnemius muscles did not show great difference in MuRF1 and atrogin1 mRNA expression. While a significant down regulation of MuRF1 was found in diaphragm muscle of transgenic mice compared to the wild type. The same trend was found for Atrogin1 but the down regulation did not reach the statistical significance for both the transgenic muscles with the placebo and those with the compound.

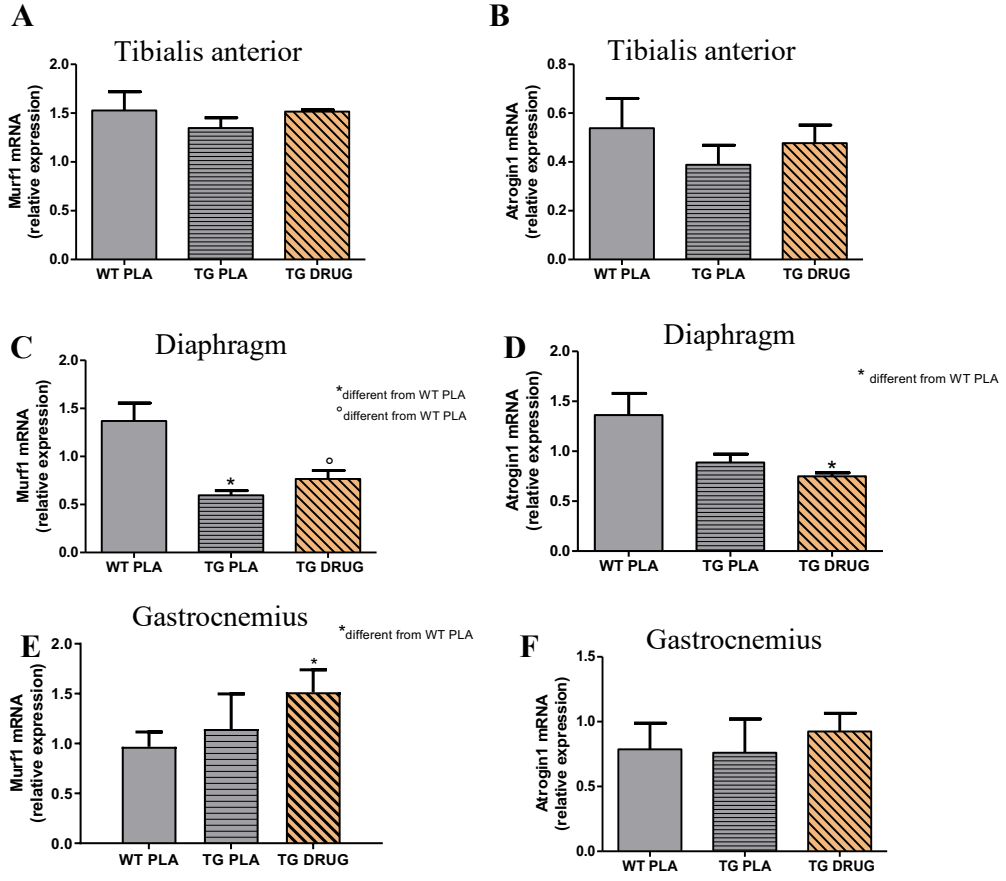

Figure 19 The graphs show the relative expression of Murf1 and Atrogin1 ubiquitin ligases from wild type and Tg(ACTA1)^{H40Y} determined by Real time PCR. The data were normalised using the GAPDH expression. The data are represented as Mean ± SD. The symbols in the figures "*" and "°" indicate a statically significant difference (p value <0.05).

Skeletal muscles from Tg (ACTA1) ^{D286G} mice showed a common downregulation of the ubiquitin proteasome markers regardless of their adaptations of muscle mass, a condition that is found common in other diseases such as many dystrophies and other myopathies (Sandri *et al*., 2013; Bühler *et al*., 2016) and that can explain the accumulation of rods in this type of myopathy. In this scenario, it is reasonable to think that dysfunctional organelles and mutated proteins cannot be eliminated leading to an accumulation of degraded proteins that will affect also the function of the muscle. According with this, it was found out that atrogin1 inactivation in zebrafish led to impairment of heart and skeletal muscle function and disruption of muscle structure without affecting early muscle development (Bühler *et al*., 2016). Some reported protease inhibitors as potential therapeutic target (Bonuccelli *et al*., 2007) to preserve muscle mass but, if continued, could be deleterious (Selsby *et al*., 2012) for the risk of the accumulation of mutated proteins that can alter the muscle structure and, so the quality of the muscle. In fact, altered quality of the proteins is one of the causes of muscle weakness as the proteins cannot form proper interactions and support their correct function.

Differently from the (ACTA1) ^{D286G} mouse model, in the (ACTA1) ^{H40Y} model the downregulation of the ubiquitin proteasome pathway is not a common mechanism shared among different muscles; in fact, only the diaphragm muscle showed the same trend in both models, i.e.the downregulation of the ubiquitin proteasome markers. This would seem in line with the large accumulation of rods in this muscle in which muscle hypertrophy could be a compensatory mechanism to contrast the large amount of nemaline rods that destroy the normal myofibrillar regions, avoiding the normal actin-myosin cross-bridge cycle and leading to muscle weakness (Lindqvist *et al*., 2013).

Unfortunately, the reason of Murf1 downregulation cannot be explained on the basis of our data.

Data on ubiquitin proteasome markers in nemaline myopathy are limited in literature. They have been analyzed in the nebulin KO model of nemaline myopathy, in the quadriceps and soleus muscles. No changes of atrogin-1 and a significant induction of Murf-1 in the quadriceps was reported (Li *et al*., 2015). These data, togheter with data collected in this thesis indicate that also the ubiquitine proteasome pathway adaptation is different between different muscles in the same model and between the same muscle

in different models. Moreover, the ubiquitin proteasome markers results obtained in the $ACTA1^{D286G}$ and $ACTA1^{H40Y}$ models do not support their role in determining the loss of muscle mass but instead they seem rather to be involved in the quality control of the proteins.

On the other hand, it is known that in muscle wasting conditions Murf1 and atrogin 1 show a transient activation (Cannavino *et al*., 2014) and therefore it can not be excluded their possible contribution in determining muscle atrophy. The determination of proteasome activity is necessary to better clarify this aspect.

Moreover, other processes, such as the authophagy, could be involved in the loss of muscle mass and it could contribute to muscle atrophy found in muscles of mice with nemaline myopathy.

Protein synthesis signalling pathway

Another pathway that was analysed in order to determine the contribution of the major pathways involved in muscle mass maintenance was the IGF-Akt pathway.
Akt stimulates protein synthesis via mTOR. mTOR forms two complexes, mTORC1 and mTORC2. TORC1 phosphorylates the S6 kinase (S6K), which in turn phosphorylates the ribosomal protein S6 stimulating protein synthesis. TORC1 also activates the eukaryotic translation initiation factor 4E (eIF4E) by phosphorylating the inhibitory eIF4E-binding proteins (4EBPs). Two proteins were evaluated in their expression levels through the analysis of the ratio among the phosphorylated active isoform and the unphosphorylated inactive isoform. In this way we could obtain the relative amount of active protein that elicit the physiological action to promote the general synthesis of protein components within the muscle fibre.

Tg (ACTA1) ^{D286G} Figure 20 shows results obtained in tibialis anterior and diaphragm muscles. As expected, in the tibialis anterior muscle the level of activation of AKT and 4EBP1 did not show substantial difference among the experimental group, meaning that synthetic pathway is maintained in its physiological activity. The same trend was observed in the diaphragm muscle except for the transgenic mice with the drug where it was found a downregulation of 4EBP1, the final target of the AKT-mTOR pathway, suggesting a potential contribution of protein synthesis reduction in determining muscle atrophy.

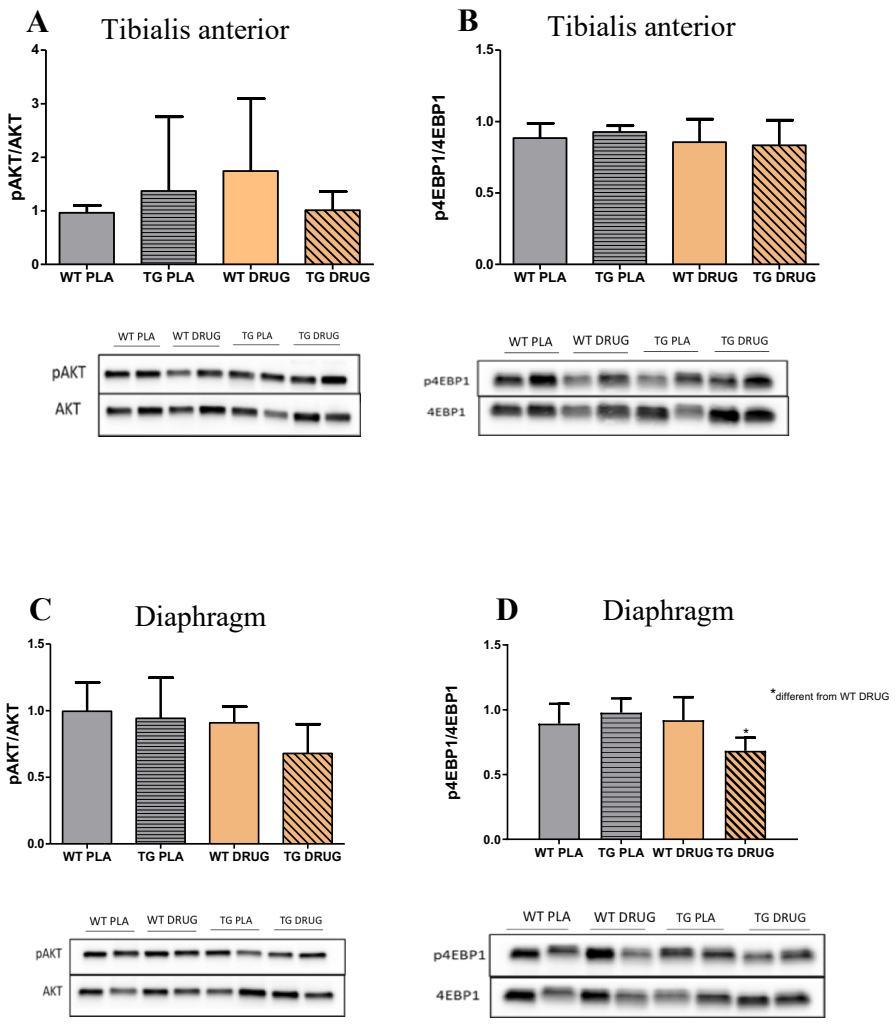

Figure 20 Western Blot determination of the protein level of AKT (A,C) and 4EBP1 (B,D) in the tibialis anterior and diaphragm from wild type and Tg ACTA1^{D286G} mice obtained normalising the phosphorylated form with the entire form of each protein. The data are represented as Mean ± SD. The symbol in the figure "*" indicates a statically significant difference (p value <0.05).

Tg (ACTA1)^{H40Y} The synthetic pathway was studied in tibialis anterior and diaphragm muscles through the activation level of AKT and 4EBP1, as in D286G mice. Results are shown in Figure 21. Phosphorylation level of both proteins were found significantly reduced in the tibialis anterior muscle of H40Y strain. As regards the diaphragm muscle no many differences were observed for both kinases. Moreover, no general effects of the drug were observed on the synthetic pathway.

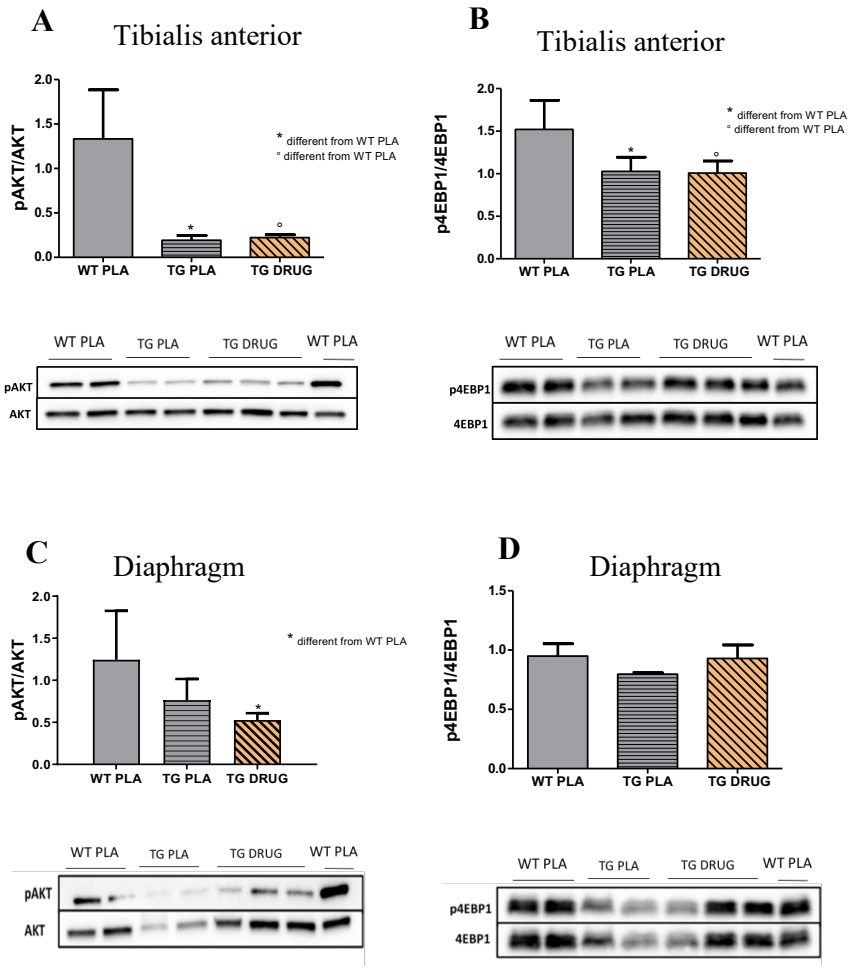

Figure 21 Western Blot determination of the protein level of Akt (A,C) and 4EBP1 (B,D) obtained normalising the phosphorylated form with the entire form of each protein from wild type and Tg(ACTA1)^{H40Y} muscles. The data are represented as Mean ± SD. The symbols in the figures "*" and "°" indicate a statically significant difference (p value <0.05).

In the diaphragm muscle from both Tg (ACTA1) ^{D286G} and Tg (ACTA1) ^{H40Y} mice no dramatic effect of nemaline myopathy and drug exposure on the markers involved in protein synthesis pathway was seen. The same for tibialis anterior muscle of Tg (ACTA1) ^{D286G} mice. Surpraisingly, the tibialis anterior muscle of Tg (ACTA1) ^{H40Y} mice, whose mass was not affected by the mutation (Figure 16) showed a strong reduction of both p-AKT/AKT and p-4EBP1/4EBP1. Considering that tibialis anterior muscle mass was preserved, it is difficult to understand the role of the synthetic pathway reduction. One possible explanation could be that tibialis anterior muscle is reprogrammed for an atrophic program whose results on the muscle mass will be appreciated in a later phase of the pathology.

Chronic treatment

CHRONIC TREATMENT

As indicated in the methods section both wild type and transgenic mice were blindly fed for 4 weeks with chow that contained either the calcium sensitizer or a placebo (chow B and chow C). All functional and molecular analyses to assess the effects of the chronic treatment were performed in the gastrocnemius muscle. This because from the "acute study" it turned out that gastrocnemius muscle was the affected muscle in both models and also because the in vivo functional determination was performed in gastrocnemius muscle.

In *vivo* functional determination

Our partner Dr. J. Gondin and his team have done the *in vivo* muscle force experiments in chronically treated mice with chow C and chow B (containing the drug and the placebo). In Figure 22 the in vivo normalized skeletal muscle force was shown.

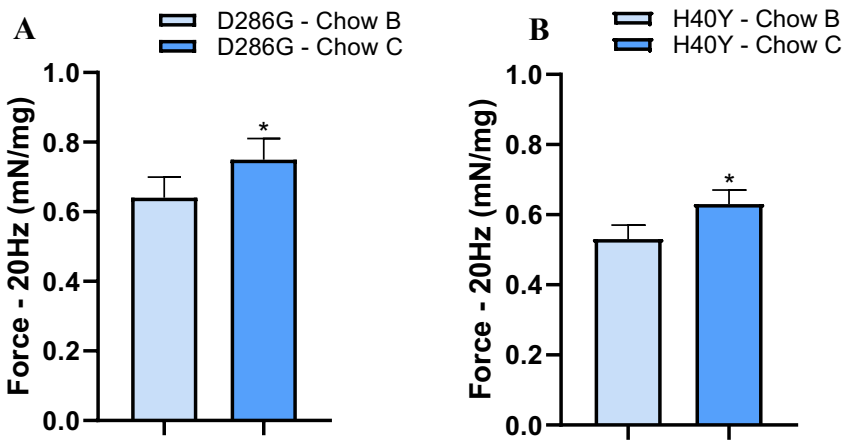

Figure 22 In vivo specific skeletal muscle force at low frequency stimulation. The graphs show the submaximal in vivo normalized skeletal muscle force of ACTA1^{D286G} (A) and ACTA1^{H40Y} (B) mice. The force was normalized on weight. The symbols in the figures "*" indicate a statically significant difference (p value <0.05).

Both ACTA1$^{(D286G)}$ and ACTA1 $^{(H40Y)}$ mice treated with chow C have shown an increase in muscle force when stimulated with a low frequency stimulation. No

changes in muscle force were observed with high frequency stimulation. These results suggest that chow C would contain the drug.

The following molecular analyses were performed on gastrocnemius muscle from the same mice used for the in vivo force determination. To better characterize the effects of the drug, the analyzes were focused on potential factors that can affect force production: muscle size, redox status /protein oxidation, Myosin Heavy Chain composition, ubiquitin proteasome markers (in light of its known effect on protein quality control).

Skeletal muscle size

To verify if single muscle fibres size has been affected by the compounds, the determination of single muscle fibres CSA on transversal gastrocnemius muscle cryosections were performed. As found in the acute study, the muscle fibers CSA (Figure 23) of gastrocnemius muscle from transgenic mice were significantly smaller than those of the wild type mice in both transgenic models (See also Figure 24 and Figure 25). In addition, no changes in CSA were found between mice received chow B and chow C, indicating no effect of the drug on single muscle size in both transgenic models.

These data confirm that the increase in force production found in muscles receiving chow C does not depend on changes in muscle mass. Experiments for the in vivo specific force determination were performed by normalizing the force on muscle weight which provides a less accurate measurement of muscle mass changes than single fibres CSA measured on muscle cryosections

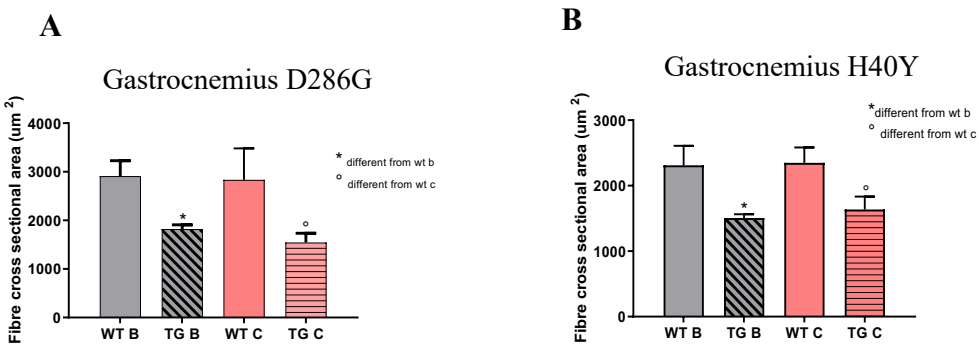

Figure 23 The graphs show the mean values fibre cross sectional area of gastrocnemius muscle from wild type and transgenic $(ACTA1)^{D286G}$ mice received both chow C and chow B (A) and of gastrocnemius muscle from wild type and knock in $(ACTA1)^{H40Y}$ mice received both chow C and chow B (B) . The data are represented as Mean ±SD. The symbols in the figures "*" and "°" indicate a statically significant difference (p value <0.05).

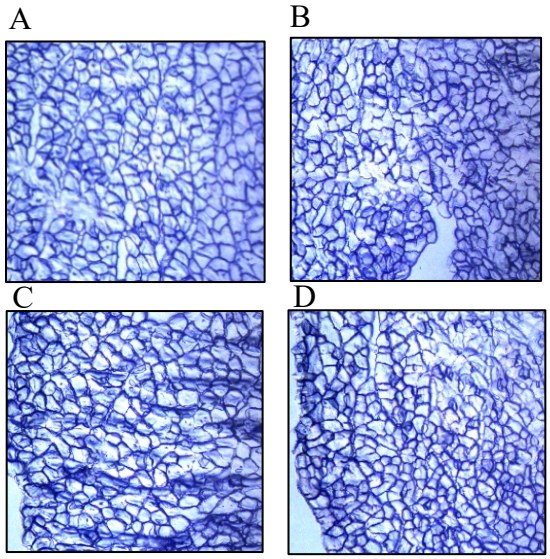

Figure 24 The images show the transverse cryosections of the gastrocnemius muscles from wild type mice with chow B (A), from Tg $ACTA1^{D286G}$ mice with chow B (B), from wild type mice with chow C (C) and from Tg $ACTA1^{D286G}$ mice with chow C (D). All the images were acquired with a 10X objective.

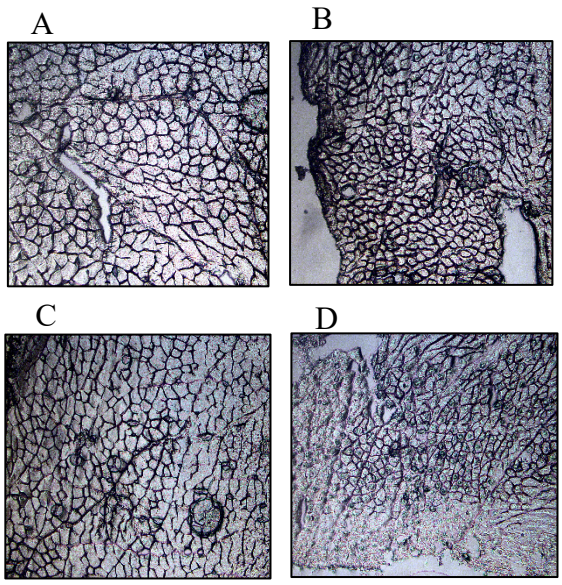

Figure 25 The images show the transverse cryosections of the gastrocnemius muscles from wild type mice with chow B (A), from Tg ACTA1^{H40Y} mice with chow B (B), from the wild type mice with chow C (C) and from Tg ACTA1^{H40Y} mice with chow C (D). All the images were acquired with a 10X objective.

Redox imbalance

Another potential factor that can influence the ability to produce muscle force is the oxidation of proteins. To determine if the transgenic animals were subjected to oxidative stress and if the chow C was able to counteract it, improving muscle force, protein carbonylation was determined. Figure 26 shows the proteins carbonylation level of gastrocnemius muscle of both wild type and ACTA1$^{(D286G)}$ transgenic mice receiving chow C and chow B.

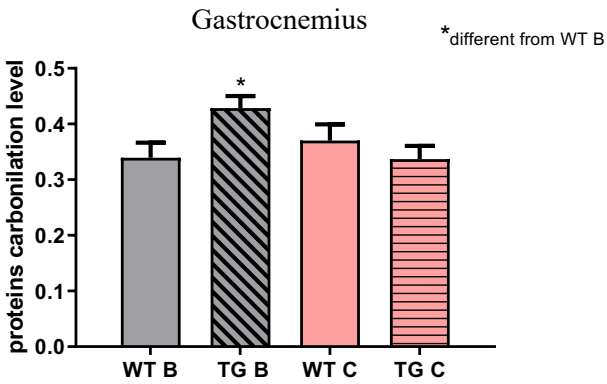

Figure 26 The graph shows oxyblot determination of the protein carbonylation level of the gastrocnemius muscle from wild type mice received chow B and C and from Tg ACTA1^{D286G} mice received chow B and C. The data are represented as Mean ± SD. The symbol in the figure "*" indicates a statically significant difference (p value <0.05).

The measurement of the levels of protein carbonyls lead to the identification of an increase of protein carbonylation level in gastrocnemius muscle of transgenic mice that received chow B, while the oxidation level of gastrocnemius muscle of transgenic mice received chow C was normal and similar to the wild type mice level. This result suggested that the chow C improved the protein quality of gastrocnemius muscle.

Furthermore, to understand the mechanism through which the treatment with chow C protected gastrocnemius muscle from oxidative stress, the expression of two key proteins involved in the antioxidant defence system, SOD1 and catalase, was determined. Results are shown in Figure 27 and indicated that the level of the catalase enzyme was increased in the transgenic mice receiving chow C supporting the hypothesis that the chow C could have an effect on the increase of the antioxidant defence system lowering the oxidized proteins, while chow B did not affect the antioxidant defence system and so the level of both catalase and SOD1 is unchanged in transgenic mice in comparison to the wild type counterpart. The lack of induction of SOD1 in mice received chow C could be due to the fact that the SOD activity is greater in the oxidative fibres (type I fibres) than in the fastest muscle fibres with low

mitochondrial volume, like type IIX and IIB fibres (Powers *et al.,* 1994) and the fibre type composition of the gastrocnemius is made up of an 80% of IIB fibres.

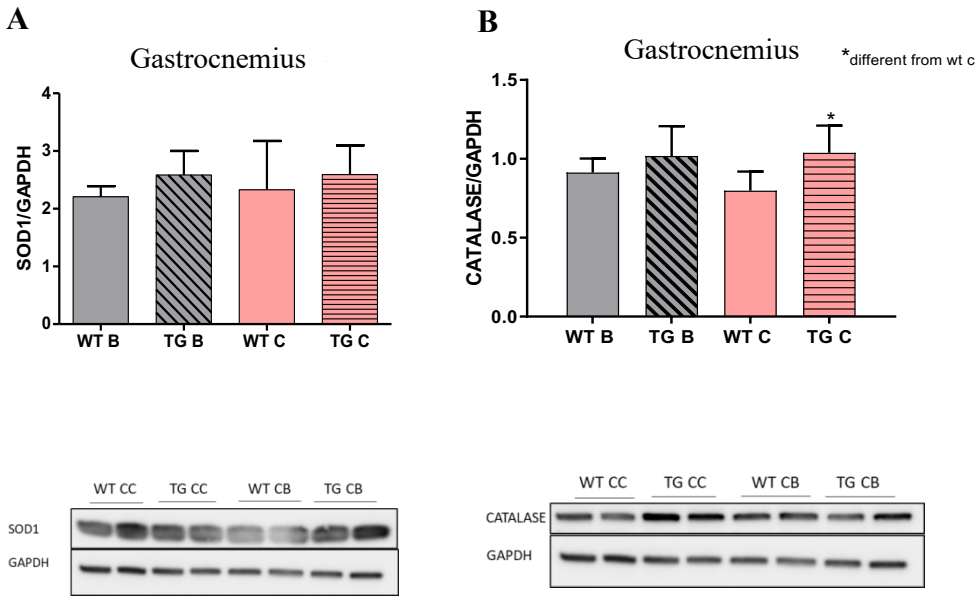

Figure 27 Western Blot determination of the protein level of SOD1 (A) and CATALASE (B) antioxidant enzymes in the gastrocnemius muscle from wild type and Tg(ACTA1)^{D286G} mice. The data are represented as Mean ± SD. The symbol in the figure "*" indicates a statically significant difference (p value <0.05).

It is known that contracting skeletal muscle generates reactive oxygen and nitrogen species (ROS and RNS) and that prolonged physical activity can cause oxidative damage to active myofibres. A lot of evidences suggest that ROS and RNS have an impact on skeletal muscle force production and that NO production shifts the force-frequency curve to the right. Low levels of ROS are essential for force production but high levels are dangerous for the cell component (Reid *et al*., 1993). As it has just said physiological level of radicals play important role in force production, this positive impact is reversed as radicals increase leading to what is called the "oxidative stress". A pro-oxidant environment in cells can damage the structure of cellular components and modify redox-sensitive molecules. Moreover, it should be said that qualitative adaptations, like for example protein post-translational modification such as

phosphorylation and oxidation, could contribute to the impairment of muscle fibre structure and function more than quantitative adaptations such as the loss of myosin and other proteins (Brocca *et al*., 2017). In fact, it was demonstrated that an antioxidant treatment restored muscle force even if it did not rescue muscle atrophy in a condition of sarcopenia (Carnio *et al*., 2014).

Therefore, these results are in line with the idea that restoring the physiological level of ROS the force production capacity of the muscle enhances.

Mitochondria parameters

Since mitochondria are the main sources of ROS production, in order to verify if chow C affected the mitochondria quality control process reducing ROS production in mice treated with chow C, the transcriptional level of the genes involved in mitochondrial dynamics was determined. Pro-fusion genes Mfn1, Mfn2 and OPA1 and pro-fission genes DRP1 and Fis1 were studied at their transcriptional level and results are shown in Figure 28.

The data obtained in ACTA1^{D286G} mice show that the level of the Mfn1 was reduced in transgenic mice both fed with chow B and chow C, while the level of Mfn2 and OPA1 did not change among all the groups.

The fission machinery was also investigated as the expression of the fission machinery is per se sufficient to cause muscle wasting in adult animals by triggering organelle dysfunction (Romanello *et al.*, 2010). Results are reported in panel D and E and no differences were found for both the profission genes DRP1 and Fis1.

In general, no great impairment of the mitochondrial parameters was found and these results are in line to what was found by Gineste *et al*., in 2013. In fact, the analysis of the PCr recovery kinetics suggested that the mitochondrial capacity was preserved in the transgenic mice ACTA1^{D286G} and that the oxidative ATP production was not impaired by this mutation (Gineste *et al.*, 2013).

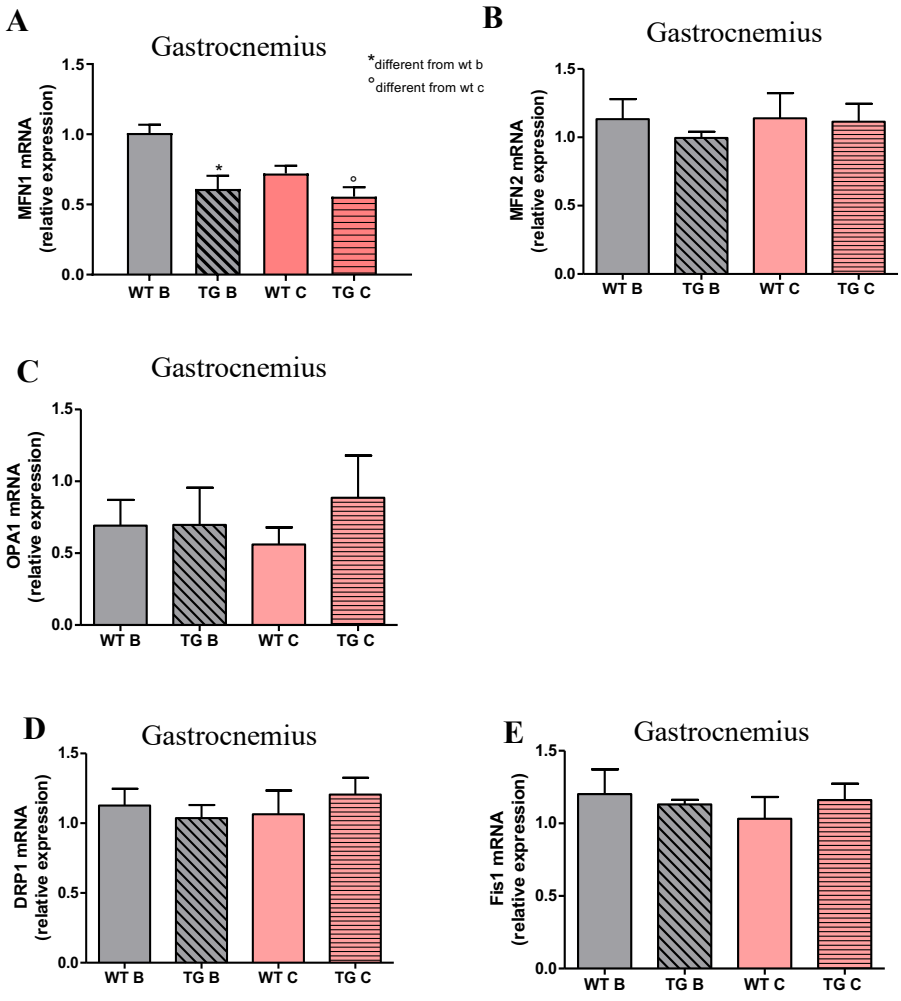

Figure 28 The graphs show the mRNA relative expression of the pro-fusion genes (MFN1, MFN2 and OPA1) (A,B,C) and pro-fission genes (DRP1 and FIS1) (D,E) of wild type and Tg(ACTA1)^{D286G} muscles. The expression was normalized to GAPDH. The data are represented as Mean ± SD. The symbols in the figure "*" and "°" indicate a statically significant difference (p value <0.05).

As regards the same factors in ACTA1^{H40Y}mice, Mfn1 was found up-regulated in both transgenic mice (both fed with chow B and chow C) compared to the wild type (Figure 29). The same trend was found for Mfn2 although statistical significance is achieved only in transgenic mice fed with chow C as well as for Fis1. DRP1 mRNA level was found unchanged among the experimental groups.

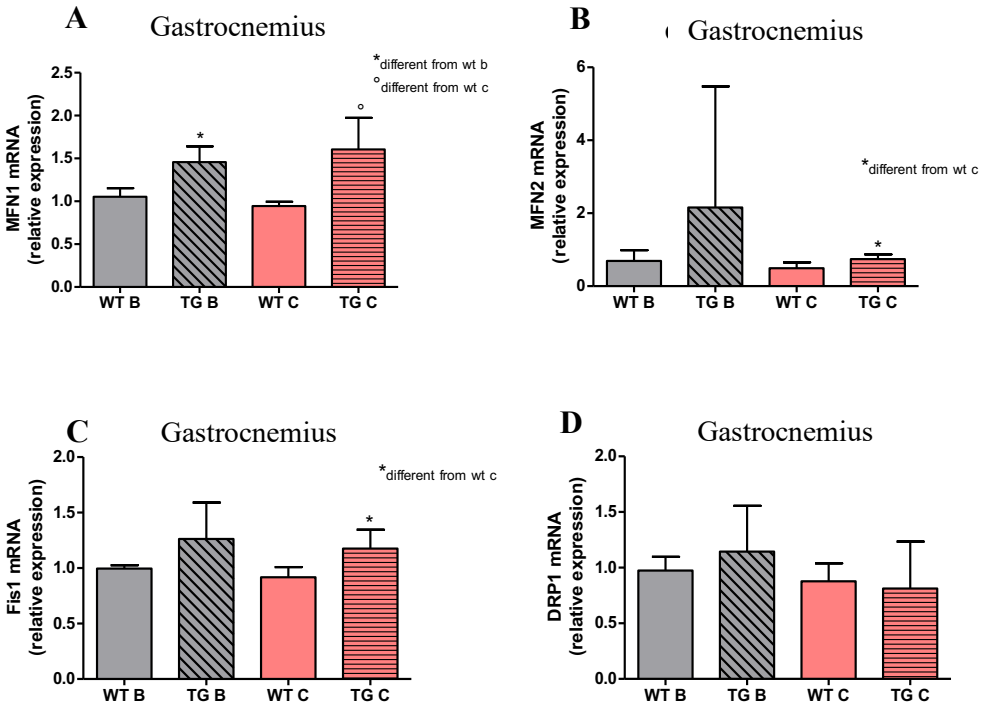

Figure 29 The figure shows the mRNA relative expression of the pro-fusion genes MFN1 (A) and MFN2 (B) and pro-fission genes DRP1 (C) and FIS1 (D) from wild type and Tg(ACTA1)^{H40Y} muscles. The expression was normalized to GAPDH. The data are represented as Mean ± SD. The symbols in the figures "*" and "°" indicate a statically significant difference (p value <0.05).

Furthermore, PGC1α, the master regulator of mitochondrial biogenesis was also investigated as a reduction of its level may let think to a reduction of the oxidative metabolism and a defect in mitochondrial biogenesis that can affect the quality of the proteins, as the mitochondria are one of the main sources of ROS. As shown in Figure 30 PGC1α did not show significant differences among groups as far as the mRNA expression for both the mice carrying the ACTA1^{D286G} mutation and those carrying the ACTA1^{H40Y} mutation.

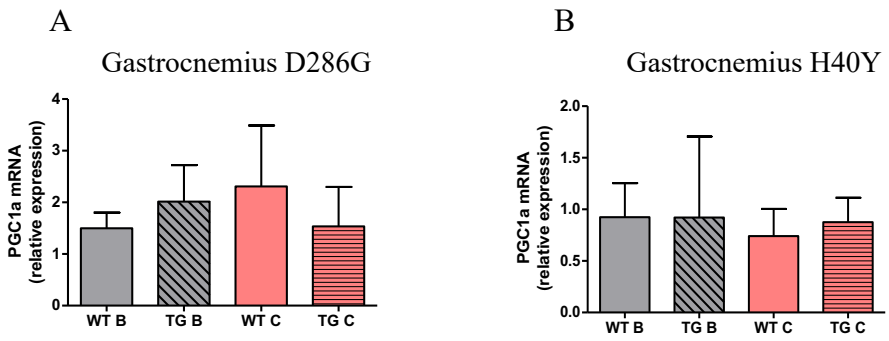

Figure 30 The graphs show the mRNA relative expression of the PGC1α gene in wild type and Tg(ACTA1)^{D286G} mice (A) and in wild type and Tg(ACTA1)^{H40Y} mice (B). The expression was normalized to GAPDH. The data are represented as Mean ± SD and the p value was set at <0.05.

There are evidences indicating the presence of mitochondrial impairment in presence of the ACTA1^{H40Y} mutation. In fact, in mice carrying the ACTA1^{H40Y} mutation subsarcolemmal mitochondria abnormally large were found (Nguyen and Hardeman, 2008) and in addition, a single case study reported mitochondrial abnormalities in a patient with nemaline myopathy (Oya *et al*., 2000). In the same line, the higher energy cost found in H40Y muscles has been hypothesized to be related to an impaired mitochondrial function (Gineste *et al*., 2013).

The concomitant increase of the profusion Mfn1 and Mfn2 mRNA level togheter with the only increase of profission Fis1 mRNA level, suggest a shift toward mitochondrial fusion in gastrocnemius muscle of transgenic mice, according with the presence of mitochondria abnormally large (Nguyen and Hardeman, 2008).

Moreover, results obtained here, did not show a significant impact of the compound C on the factors controlling mitochondrial dynamics, in comparison with the compound B, suggesting that the normalization of protein oxidation level found with the coumpound C (Figure 26) was not due to an improvement of mitochondrial quality through the mitochondrial dynamics process.

Ubiquitin proteasome markers

The ubiquitin proteasome system is crucial in removing carbonylated proteins (Stankovic-Valentin and Melchior, 2018). To verify if the reduction of carbonylated proteins level found in ACTA1^{D286G} mice treated with chow C was due to an increase of the proteasome activity, MuRF1 and atrogin1 mRNA expression (the major ubiquitin ligases) was determined. The same markers were explored also in the ACTA1^{H40Y}mice.

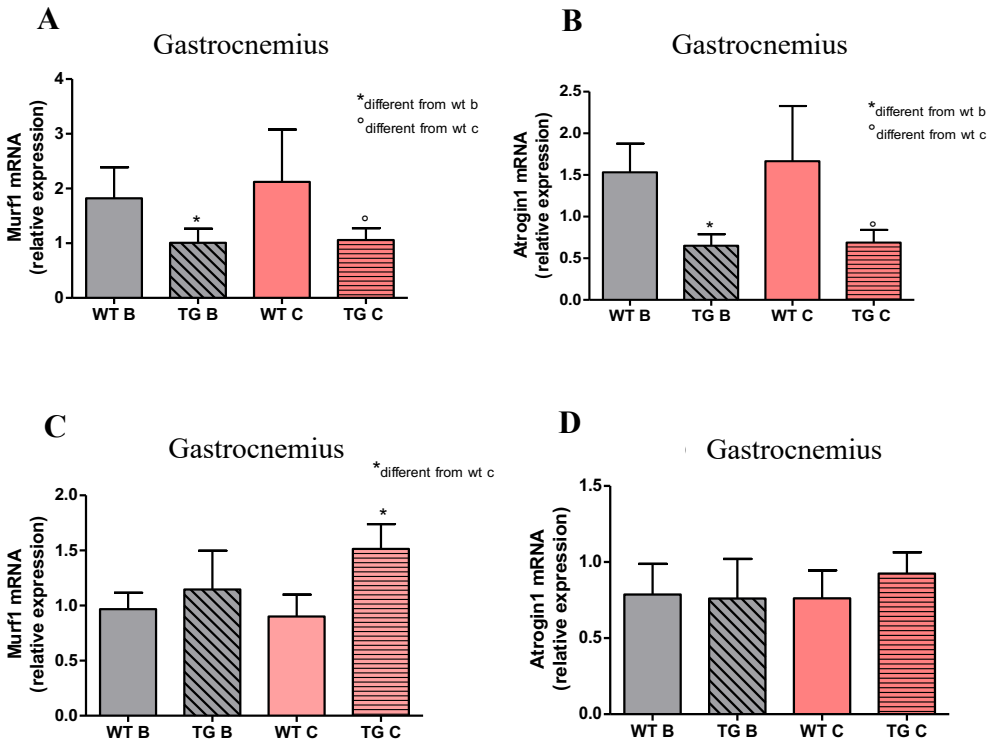

Figure 31 Relative expression of Murf1 and Atrogin1 ubiquitin ligases determined by Real time PCR in the gastrocnemius muscle from wild type and Tg(ACTA1)^{D286G} mice (A, B) and in the gastrocnemius muscle from wild type and Tg(ACTA1)^{H40Y} mice (C,D). The data were normalised using the GAPDH expression. The data are represented as Mean ± SD. The symbols in the figures "*" and "°" indicate a statically significant difference (p value <0.05).

As shown in Figure 31 the level of the expression of both MuRF1 and atrogin1 was lower in the ACTA1^{D286G} mice in comparison to the wild type (panel A and B) and no affected in the ACTA1^{H40Y}mice (panel C and D).

In ACTA1^{D286G} mice model no effects of the compounds were observed. These results suggested no contribution of ubiquitin proteasome system in removing the oxidized proteins in gastrocnemius of ACTA1^{D286G} mice treated with chow C. Gastrocnemius muscle of ACTA1^{H40Y}mice fed with chow C showed an increase of MuRF1 mRNA level. Unfortunatly, the evaluation of the redox status in ACTA1^{H40Y} mice is in progress and it is not possible to establish wheter the increase of MuRF1 could be involved in the removal of carbonylated proteins in this transgenic mouse model. The relevance of the ubiquitine proteasome markers in the two transgenic mouse models has already been discussed above (see pag.74).

Myosin/actin ratio

One of the parameters that could cause the loss of force is the alteration of the myosin actin ratio, as myosin and actin, the two sarcomere contractile proteins, should be in the right proportion in order to determine the force by the proper actin myosin binding. This was studied in ACTA1^{D286G} mice but not revealed a preferential loss of actin or myosin in both the transgenic muscles receiving chow B and C (Figure 32).

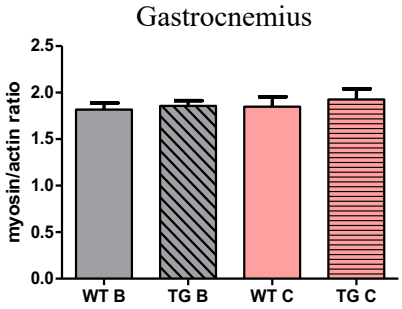

Figure 32 The graph shows the myosin/actin ratio among four different groups: wild type received both chow B and chow C and transgenic $(ACTA1)^{D286G}$ mice received both chow B and chow C. No differences were found. The data are represented as Mean ± SD and the p value was set at <0.05.

This is in agreement with Ochala *et al.,* 2012 that showed no changes of the myosin actin ratio indicating that the relative content of actin was unaffected in D286G mice (Ochala *et al*., 2012).

MHC isoforms composition

Alterations in muscle force can occur not only via changes in muscle quantity but also via changes in muscle quality. As illustrated in the introduction section, skeletal muscles contain different fiber types and a simple shift in the type of MHC isoform expressed in the fibre will produce different tissue level velocity and tension (force per CSA) characteristics, as faster contracting MHCs (I < IIA < IIX) produce more tension. In order to understand if the MHC isoforms shift contribute to the increase in force observed in gastrocnemius muscle of mice that received the compound C, the MHC isoforms composition was determined in $ACTA1^{D286G}$ mice and results are shown in Figure 33.

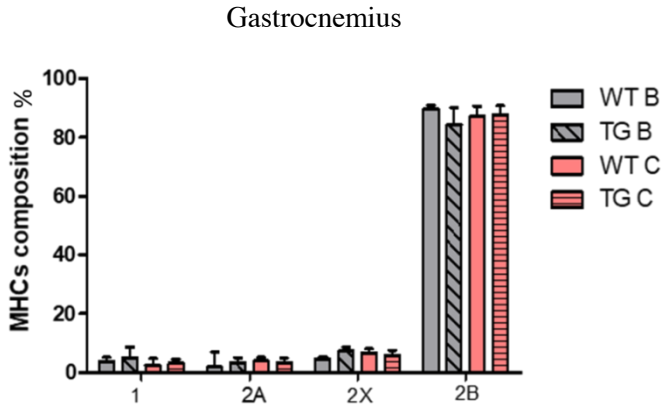

Figure 33 The graph shows the Myosin Heavy Chains composition of the gastrocnemius muscle from wild type mice received chow B and chow C and from transgenic mice $(ACTA1)^{D286G}$ received chow B and C. The data are represented as Mean ± SD. The p value was set at < 0.05.

According with the literature, in gastrocnemius muscle all four MHC isoforms were detected with the fast isoforms 2B being dominant ones. No changes were observed in MHC isoforms content among the experimental group.

Despite an increase in the number of oxidative fibers has been shown in the Soleus muscle of the $Acta1^{H40Y}$ mouse model of nemaline (Nguyen *et al*., 2011) and of the Nebuline cKO model (Li *et al*., 2015), the absence of fiber-type composition shift has been also documented in muscles of the TnI_{slow}-αTm_{slow} (Met9Arg) nemaline model (Corbett *et al*., 2001). Our findings in the $ACTA1^{D286G}$ model did not show any shift in MHC isoforms. This is in agreement with PGC1α gene expression analysis that did not reveal changes in this gene (Figure 30) that is thought to be important in fibre-type switching.

Conclusion

Nemaline Myopathy is a rare genetic disease with an incidence of 1:50000 but, although rare, it is the most common among congenital myopathies (Romero *et al*., 2013).

This project started in order to test in Nemaline Myopathy disease the efficacy of a compound (calcium sensitizer) that obtained the fast track designation and the orphan drug status by FDA for another muscular disease. Till now no therapeutic treatment excepts for mechanical ventilation and nasogastric feeding exists for these patients (Wallgren-Pettersson *et al*., 2011) and this study aimed to understand if this drug was useful also for the treatment of the nemaline myopathy improving its symptoms.

The project consisted of two parts, the first part was focused on the analyses aimed at understanding the effects of the acute administration, one injection of the compound, on skeletal muscles. The second part was focused to test the effects of the chronic administration of the compound, 4 weeks, performed as a double-blind study, on functional, molecular and cellular muscular adaptations.

In the acute study no effect of the compound has been seen both in the wild type and in the two transgenic mice with nemaline myopathy, the Acta1^{D286G} and the Acta1^{H40Y}.

Samples from this phase were used to analyse the consequences of the mutation on skeletal muscles, in order to clarify the pathophysiology of the Nemaline Myopathy.

A different skeletal muscles response to the Nemaline Myopathy disease has been found both in the Tg (ACTA1)^{D286G} and Tg (ACTA1)^{H40Y} models both in terms of muscle size and parameters involved in its maintenance.

Muscle size of the tibialis anterior muscle was found preserved in both transgenic models, the diaphragm muscle resulted atrophic in the Tg (ACTA1)^{D286G} and displayed hypertrophy of slow fibers in the Tg (ACTA1)^{H40Y} model while the gastrocnemius muscle displayed atrophy in both models.

In the same way, markers of ubiquitine proteasome showed a different adaptation in the two models, in particular their under-regulation in Tg (ACTA1)^{D286G} muscles suggest a possible role in determining accumulation of rods.

The chronic study was centred on the analyses of the gastrocnemius muscle, a muscle affected by the pathology in both transgenic models. Both wild type and transgenic mice were blindly fed with chow that contained either the calcium sensitizer or a placebo (chow B and chow C).

The chronic administration of the compound C enhanced the force-production capacity both in ACTA1$^{(D286G)}$ and ACTA1 $^{(H40Y)}$ mice. To better characterize the effects of the drug, the molecular analyzes were focused on potential factors that can affect force production: muscle size, redox status /protein oxidation, Myosin Heavy Chain composition, ubiquitin proteasome markers (in light of its known effect on protein quality control). The chronic administration of the compound C was neither associated with effects on muscle size nor with effects on MHC isoforms composition. Interestingly a normalization of the protein oxidation level through the increase of antioxidant enzymes was associated with the administration of the coumpound C suggesting that the improvement of the protein quality could contribute to the enhancement of force production.

As it was a double-blind study, relying on data obtained, we can suppose that the compound C contains the drug. The effectiveness of the drug in improving the in vivo muscle force production and the protein quality are very encouraging results that could lead to have a new potential treatment to counteract muscle weakness in this rare disease improving the quality of life of these patients: Nevertheless, further analyses are needed to assess its efficacy and safety.

References

1. Agrawal PB, Strickland CD, Midgett C, Morales A, Newburger DE, Poulos MA, Tomczak KK, Ryan MM, Iannaccone ST, Crawford TO, Laing NG, Beggs AH "Heterogeneity of nemaline myopathy cases with skeletal muscle alpha-actin gene mutations" Ann Neurol. 2004;56(1):86-96.
2. Alloatti G, Antonutto G, Bottinelli R, Cevese A, Concu A, Conti F, De Lorenzo A, di Prampero PE, Fanò G, Fantin G, Favilla M, Felici F, Fulle S, Gravante G, Leone D, Luppino G, Manasseri L, Orizio C, Perini R, Pettorossi VE, Ruggeri P, Santacroce L, Scarnati E, di Vettimo PS, Squatrito S, Veicsteinas A "Fisiologia dell'uomo" edi-ermes editor 2002.
3. Bodine SC, Latres E, Baumhueter S, Lai VK, Nunez L, Clarke BA, Poueymirou WT, Panaro FJ, Na E, Dharmarajan K, Pan ZQ, Valenzuela DM, DeChiara TM, Stitt TN, Yancopoulos GD, Glass DJ "Identification of ubiquitin ligases required for skeletal muscle atrophy" Science. 2001 Nov 23;294(5547):1704-8.
4. Bonuccelli G, Sotgia F, Capozza F, Gazzerro E, Minetti C, Lisanti MP "Localized treatment with a novel FDA-approved proteasome inhibitor blocks the degradation of dystrophin and dystrophin-associated proteins in mdx mice" Cell Cycle. 2007 May 15;6(10):1242-8.
5. Brigelius-Flohé R "Tissue-specific functions of individual glutathione peroxidases" Free Radic Biol Med. 1999 Nov;27(9-10):951-65.
6. Brocca L, McPhee JS, Longa E, Canepari M, Seynnes O, De Vito G, Pellegrino MA, Narici M, Bottinelli R "Structure and function of human muscle fibres and muscle proteome in physically active older men" J Physiol. 2017 Jul 15;595(14):4823-4844.
7. Brocca L, Pellegrino MA, Desaphy JF, Pierno S, Camerino DC, Bottinelli R "Is oxidative stress a cause or consequence of disuse muscle atrophy in mice? A proteomic approach in hindlimb-unloaded mice" Exp Physiol. 2010 Feb;95(2):331-50.
8. Bruno C, Minetti C "Congenital myopathies" Curr Neurol Neurosci Rep. 2004 Jan;4(1):68-73.

9. Bühler A, Kustermann M, Bummer T, Rottbauer W, Sandri M, Just S "Atrogin-1 Deficiency Leads to Myopathy and Heart Failure in Zebrafish" Int J Mol Sci. 2016 Jan 30;17(2).
10. Cannavino J, Brocca L, Sandri M, Bottinelli R, Pellegrino MA "PGC1-α over-expression prevents metabolic alterations and soleus muscle atrophy in hindlimb unloaded mice" J Physiol. 2014 Oct 15;592(20):4575-89.
11. Carnio S, LoVerso F, Baraibar MA, Longa E, Khan MM, Maffei M, Reischl M, Canepari M, Loefler S, Kern H, Blaauw B, Friguet B, Bottinelli R, Rudolf R, Sandri M "Autophagy impairment in muscle induces neuromuscular junction degeneration and precocious aging" Cell Rep. 2014 Sep 11;8(5):1509-21.
12. Cassandrini D, Trovato R, Rubegni A, Lenzi S, Fiorillo C, Baldacci J, Minetti C, Astrea G, Bruno C, Santorelli FM; Italian Network on Congenital Myopathies. "Congenital myopathies: clinical phenotypes and new diagnostic tools" Ital J Pediatr 2017 Nov 15;43(1):101.
13. Chan C, Fan J, Messer AE, Marston SB, Iwamoto H, Ochala J "Myopathy-inducing mutation H40Y in ACTA1 hampers actin filament structure and funct ion" Biochim Biophys Acta. 2016 Aug;1862(8):1453-8.
14. Clarkson E, Costa CF, Machesky LM "Congenital myopathies: diseases of the actin cytoskeleton" J Pathol. 2004 Nov; 204(4) 407-17-
15. Cohen-Kaplan V, Livneh I, Avni N, Cohen-Rosenzweig C, Ciechanover A "The ubiquitin-proteasome system and autophagy: Coordinated and independent activities" Int J Biochem Cell Biol. 2016 Oct;79:403-418.
16. Cokorinos EC, Delmore J, Reyes AR, Albuquerque B, Kjøbsted R, Jørgensen NO, Tran JL, Jatkar A, Cialdea K, Esquejo RM, Meissen J, Calabrese MF, Cordes J, Moccia R, Tess D, Salatto CT, Coskran TM, Opsahl AC, Flynn D, Blatnik M, Li W, Kindt E, Foretz M, Viollet B, Ward J, Kurumbail RG, Kalgutkar AS, Wojtaszewski JFP, Cameron KO, Miller RA "Activation of Skeletal Muscle AMPK Promotes Glucose Disposal and Glucos e Lowering in Non-humanPrimates and Mice" Cell Metab. 2017 May 2;25(5):1147-1159.e10.

17. Conen PE, Murphy EG, Donohue WL “Light and electron microscopic studies of myogranules” Can Med Assoc J. 1963 Nov 9;89:983-6.
18. Corbett MA, Robinson CS, Dunglison GF, Yang N, Joya JE, Stewart AW, Schnell C, Gunning PW, North KN, Hardeman EC “A mutation in alpha-tropomyosin(slow) affects muscle strength, maturation and hypertrophy in a mouse model for nemaline myopathy” Hum Mol Genet. 2001 Feb 15;10(4):317-28.
19. Crawford K, Flick R, Close L, Shelly D, Paul R, Bove K, Kumar A, Lessard J “Mice lacking skeletal muscle actin show reduced muscle strength and growth deficits and die during the neonatal period.” Mol Cell Biol. 2002 Aug;22(16):5887-96.
20. Culotta VC, Yang M, O'Halloran TV “Activation of superoxide dismutases: putting the metal to the pedal” Biochim Biophys Acta. 2006 Jul;1763(7):747-58.
21. Dalle-Donne I, Rossi R, Colombo R, Giustarini D, Milzani A “Biomarkers of oxidative damage in human disease” Clin Chem. 2006 Apr; 52(4):601-23.
22. de Winter JM, Buck D, Hidalgo C, Jasper JR, Malik FI, Clarke NF, Stienen GJ, Lawlor MW, Beggs AH, Ottenheijm CA, Granzier H “Troponin activator augments muscle force in nemaline myopathy patients wit h nebulin mutations” J Med Genet. 2013 Jun;50(6):383-92.
23. de Winter JM, Joureau B, Sequeira V, Clarke NF, van der Velden J, Stienen GJ, Granzier H, Beggs AH, Ottenheijm CA “Effect of levosimendan on the contractility of muscle fibers from nemaline myopathy patients with mutations in the nebulin gene” Skelet Muscle 2015 Apr 28; 5:12.
24. Dominguez R, Holmes KC “Actin structure and function” Annu Rev Biophys 2011;40:169-86.
25. Foletta VC, White LJ, Larsen AE, Léger B, Russell AP “The role and regulation of MAFbx/atrogin-1 and MuRF1 in skeletal muscle atrophy” Pflugers Arch. 2011 Mar;461(3):325-35.
26. Friedman B, Simpson K, Tesi-Rocha C, Zhou D, Palmer CA, Suchy SF “Novel large deletion in the ACTA1 gene in a child with autosomal recessive nemaline myopathy” Neuromuscul Disord. 2014 Apr;24(4):331-4.

27. Frontera WR, Ochala J. "Skeletal muscle: a brief review of structure and function" Calcif Tissue Int. 2015;96(3):183-95.
28. Gineste C, Duhamel G, Le Fur Y, Vilmen C, Cozzone PJ, Nowak KJ, Bendahan D, Gondin J "Multimodal MRI and (31) P-MRS investigations of the ACTA1(Asp286Gly) mouse model of nemaline myopathy provide evidence of impaired in vivo muscle function, altered muscle structure and disturbed energy metabolism" PLoS One. 2013;8(8):e72294.
29. Gineste C, Le Fur Y, Vilmen C, Le Troter A, Pecchi E, Cozzone PJ, Hardeman EC, Bendahan D, Gondin J "Combined MRI and ^{31}P-MRS investigations of the ACTA1(H40Y) mouse model of nemaline myopathy show impaired muscle function and altered energy metabolism" PLoS One. 2013 Apr 16;8(4): e61517.
30. Granit R, Henatsch HD, Steg G "Tonic and phasic ventral horn cells differentiated by post-tetanic potentiation in cat extensors" Acta Physiol Scand 1956; 37: 114-126.
31. Greising SM, Gransee HM, Mantilla CB, Sieck GC "Systems biology of skeletal muscle: fiber type as an organizing principle" Wiley Interdiscip Rev Syst Biol Med. 2012;4(5):457-73.
32. Hales KG, Fuller MT "Developmentally regulated mitochondrial fusion mediated by a conserved, novel, and predicted GTPase" Cell. 1997 Jul 11;90(1):121-9.
33. Halliwell B "Free radicals and antioxidants: a personal view" Nutr Rev. 1994 Aug;52(8 Pt 1):253-65.
34. Halliwell B and Gutteridge, J. Free radicals in biology and medicine. Oxford Press; Oxford: 2007. p. 936
35. Hardie DG "AMP-activated protein kinase: a cellular energy sensor with a key role in metabolic disorders and in cancer" Biochem Soc Trans. 2011 Jan;39(1):1-13.
36. Hardie DG "AMPK—Sensing Energy while Talking to Other Signaling Pathways" Cell Metabolism 2014 Dec 2;20(6):939-52.

37. He L, He T, Farrar S, Ji L, Liu T, Ma X "Antioxidants Maintain Cellular Redox Homeostasis by Elimination of Reactive Oxygen Species" Cell Physiol Biochem 2017; 44(2):532-553.
38. Henneman E, Clamann HP, Gillies JD, Skinner RD "Rank order of motoneurons within a pool: law of combination" J Neurophysiol 1974; 37: 1338 –1349.
39. Hwang PM, Sykes BD. "Targeting the sarcomere to correct muscle function" Nat Rev Drug Discov. 2015;14(5):313-28.
40. Ilkovski B, Cooper ST, Nowak K, Ryan MM, Yang N, Schnell C, Durling HJ, Roddick LG, Wilkinson I, Kornberg AJ, Collins KJ, Wallace G, Gunning P, Hardeman EC, Laing NG, North KN "Nemaline myopathy caused by mutations in the muscle alpha-skeletal-actin gene" Am J Hum Genet. 2001 Jun;68(6):1333-43. Epub 2001 Apr 27
41. Ishihara N, Eura Y, Mihara K. "Mitofusin 1 and 2 play distinct roles in mitochondrial fusion reactions via GTPase activity" J Cell Sci. 2004 Dec 15;117(Pt 26):6535-46.
42. Johnston JJ, Kelley RI, Crawford TO, Morton DH, Agarwala R, Koch T, Schäffer AA, Francomano CA, Biesecker LG "A novel nemaline myopathy in the Amish caused by a mutation in troponin T1" Am J Hum Genet. 2000 Oct;67(4):814-21.
43. Kabsch W, Mannherz HG, Suck D, Pai EF, Holmes KC. "Atomic structure of the actin: DNase I complex" Nature. 1990;347(6288):37-44.
44. Kabsch W, Vandekerckhove J." "Structure and function of actin" Annu Rev Biophys Biomol Struct. 1992; 21:49-76.
45. Kirkman HN, Gaetani GF "Mammalian catalase: a venerable enzyme with new mysteries" Trends Biochem Sci. 2007 Jan;32(1):44-50.
46. Laemmli UK "Cleavage of structural proteins during the assembly of the head of bacteriophage T4" Nature. 1970 Aug 15;227(5259):680-5.
47. Laing NG, Dye DE, Wallgren-Pettersson C, Richard G, Monnier N, Lillis S, Winder TL, Lochmüller H, Graziano C, Mitrani-Rosenbaum S, Twomey D, Sparrow JC, Beggs AH, Nowak KJ "Mutations and polymorphisms of the skeletal muscle alpha-actin gene (ACTA1)" Hum Mutat. 2009;30(9):1267-77.

48. Li F, Buck D, De Winter J, Kolb J, Meng H, Birch C, Slater R, Escobar YN, Smith JE 3rd, Yang L, Konhilas J, Lawlor MW, Ottenheijm C, Granzier HL "Nebulin deficiency in adult muscle causes sarcomere defects and muscle-type-dependent changes in trophicity: novel insights in nemaline myopathy" Hum Mol Genet. 2015 Sep 15;24(18):5219-33.
49. Liesa M, Palacín M, Zorzano A "Mitochondrial dynamics in mammalian health and disease" Physiol Rev. 2009 Jul;89(3):799-845.
50. Lindqvist J, Cheng AJ, Renaud G, Hardeman EC, Ochala J "Distinct Underlying Mechanisms of Limb and Respiratory Muscle Fiber Weaknessess in Nemaline Myopathy" J Neuropathol Exp Neurol 2013 Jun; 72(6):472-81.
51. Lowry OH, Rosebrough NJ, Farr AL, Randall RJ "Protein measurement with the Folin phenol reagent" J Biol Chem. 1951 Nov;193(1):265-75.
52. Malfatti E, Romero NB "Nemaline myopathies: State of the art" Rev Neurol (Paris). 2016 Oct;172(10):614-619.
53. Manning BD, Cantley LC "AKT/PKB signaling: navigating downstream" Cell. 2007 Jun 29;129(7):1261-74.
54. McCord JM, Fridovich I "Superoxide dismutase. An enzymic function for erythrocuprein (hemocuprein)" J Biol Chem. 1969 Nov 25;244(22):6049-55.
55. Milan G, Romanello V, Pescatore F, Armani A, Paik JH, Frasson L, Seydel A, Zhao J, Abraham R, Goldberg AL, Blaauw B, DePinho RA, Sandri M "Regulation of autophagy and the ubiquitin-proteasome system by the FoxO transcriptional network during muscle atrophy" Nat Commun. 2015; 6:6670.
56. Moreau-Le Lan S, Aller E, Calabria I, Gonzalez-Tarancon L, Cardona-Gay C, Martinez-Matilla M, Aparisi MJ, Selles J, Sagath L, Pitarch I, Muelas N, Cervera JV, Millan JM, Pedrola L "New mutations found by Next-Generation Sequencing screening of Spanish patients with Nemaline Myopathy" PLoS One. 2018 Dec 5;13(12):e0207296.
57. Nguyen MA, Hardeman EC "Mouse models for thin filament disease" Adv Exp Med Biol. 2008; 642: 66-77.
58. Nguyen MA, Joya JE, Kee AJ, Domazetovska A, Yang N, Hook JW, Lemckert FA, Kettle E, Valova VA, Robinson PJ, North KN, Gunning PW, Mitchell CA, Hardeman EC "Hypertrophy and dietary tyrosine ameliorate the phenotypes of

a mouse model of severe nemaline myopathy" Brain. 2011 Dec;134(Pt 12):3516-29.

59. North KN, Laing NG, Wallgren-Pettersson C. "Nemaline myopathy: current concepts. The ENMC International Consortium and Nemaline Myopathy" J Med Genet. 1997 Sep;34(9):705-13.
60. Nowak KJ, Ravenscroft G, Laing NG "Skeletal muscle α-actin diseases (actinopathies): pathology and mechanisms" Acta Neuropathol. 2013;125(1):19-32.
61. Nowak KJ, Wattanasirichaigoon D, Goebel HH, Wilce M, Pelin K, Donner K, Jacob RL, Hübner C, Oexle K, Anderson JR, Verity CM, North KN, Iannaccone ST, Müller CR, Nürnberg P, Muntoni F, Sewry C, Hughes I, Sutphen R, Lacson AG, Swoboda KJ, Vigneron J, Wallgren-Pettersson C, Beggs AH, Laing NG "Mutations in the skeletal muscle alpha-actin gene in patients with actin myopathy and nemaline myopathy" Nat Genet. 1999;23(2):208-12.
62. Ochala J "Ca2+ sensitizers: An emerging class of agents for counterbalancing weakness in skeletal muscle diseases?" Neuromuscul Disord. 2010 Feb;20(2):98-101.
63. Ochala J, Ravenscroft G, Laing NG, Nowak KJ "Nemaline myopathy-related skeletal muscle α-actin (ACTA1) mutation, Asp286Gly, prevents proper strong myosin binding and triggers muscle weakness" PLoS One. 2012;7(9):e45923.
64. Ochala J, Ravenscroft G, McNamara E, Nowak KJ, Iwamoto H "X-ray recordings reveal how a human disease-linked skeletal muscle α-actin mutation leads to contractile dysfunction" J Struct Biol. 2015 Dec;192(3):331-335.
65. Otera H, Wang C, Cleland MM, Setoguchi K, Yokota S, Youle RJ, Mihara K "Mff is an essential factor for mitochondrial recruitment of Drp1 during mitochondrial fission in mammalian cells" J Cell Biol. 2010 Dec 13;191(6):1141-58.
66. Oya Y, Segawa M, Ogawa M, Goto Y, Nonaka I, Kawai M "Congenital nemaline myopathy with mitochondrial abnormalities. An adult case report" Rinsho Shinkeigaku 2000 May; 40(5): 452-8.

67. Palmer CS, Osellame LD, Laine D, Koutsopoulos OS, Frazier AE, Ryan MT "MiD49 and MiD51, new components of the mitochondrial fission machinery" EMBO Rep. 2011 Jun;12(6):565-73.
68. Pardo CA, Xu Z, Borchelt DR, Price DL, Sisodia SS, Cleveland DW. "Superoxide dismutase is an abundant component in cell bodies, dendrites, and axons of motor neurons and in a subset of other neurons" Proc Natl Acad Sci U S A. 1995 Feb 14;92(4):954-8.
69. Pellegrino MA, Canepari M, Rossi R, D'Antona G, Reggiani C, Bottinelli R." Orthologous myosin isoforms and scaling of shortening velocity with body size in mouse, rat, rabbit and human muscles" J Physiol. 2003;546(Pt 3):677-89.
70. Pollesello P, Papp Z, Papp JG "Calcium sensitizers: What have we learned over the last 25 years?" Int J Cardiol. 2016 Jan 15;203:543-8.
71. Powers SK, Criswell D, Lawler J, Ji LL, Martin D, Herb RA, Dudley G "Influence of exercise and fiber type on antioxidant enzyme activity in rat skel etal muscle" Am J Physiol. 1994 Feb;266(2 Pt 2):R375-80.
72. Puigserver P, Spiegelman BM "Peroxisome proliferator-activated receptor-gamma coactivator 1 alpha (PGC-1 alpha): transcriptional coactivator and metabolic regulator" Endocr Rev. 2003 Feb;24(1):78-90.
73. Puigserver P, Wu Z, Park CW, Graves R, Wright M, Spiegelman BM "A cold-inducible coactivator of nuclear receptors linked to adaptive thermogenesis" Cell. 1998 Mar 20;92(6):829-39.
74. Ravenscroft G, Jackaman C, Bringans S, Papadimitriou JM, Griffiths LM, McNamara E, Bakker AJ, Davies KE, Laing NG, Nowak KJ." Mouse models of dominant ACTA1 disease recapitulate human disease and provide insight into therapies" Brain. 2011 Apr;134(Pt 4):1101-15
75. Ravenscroft G, Jackaman C, Sewry CA, McNamara E, Squire SE, Potter AC, Papadimitriou J, Griffiths LM, Bakker AJ, Davies KE, Laing NG, Nowak KJ "Actin nemaline myopathy mouse reproduces disease, suggests other actin disease phenotypes and provides cautionary note on muscle transgene expression" PLoS One. 2011;6(12):e28699.

76. Reid MB, Khawli FA, Moody MR "Reactive oxygen in skeletal muscle. III. Contractility of unfatigued muscle" J Appl Physiol (1985). 1993 Sep;75(3):1081-7.
77. Romanello V, Guadagnin E, Gomes L, Roder I, Sandri C, Petersen Y, Milan G, Masiero E, Del Piccolo P, Foretz M, Scorrano L, Rudolf R, Sandri M "Mitochondrial fission and remodelling contributes to muscle atrophy" EMBO J. 2010 May 19;29(10):1774-85.
78. Romanello V, Sandri M "Mitochondrial Quality Control and Muscle Mass Maintenance" Front Physiol. 2016 Jan 12;6:422.
79. Romero NB, Clarke NF "Congenital myopathies" Handb Clin Neurol. 2013;113:1321-36.
80. Romero NB, Sandaradura SA, Clarke NF "Recent advances in nemaline myopathy" Curr Opin Neurol. 2013 Oct;26(5):519-26.
81. Ryan MM, Schnell C, Strickland CD, Shield LK, Morgan G, Iannaccone ST, Laing NG, Beggs AH, North KN "Nemaline myopathy: a clinical study of 143 cases" Ann Neurol. 2001 Sep;50(3):312-20.
82. Salvador A, Sousa J, Pinto RE. "Hydroperoxyl, superoxide and pH gradients in the mitochondrial matrix: a theoretical assessment" Free Radic Biol Med. 2001 Nov 15;31(10):1208-15.
83. Sandri M "Autophagy in skeletal muscle" FEBS Lett. 2010 Apr 2;584(7):1411-6.
84. Sandri M, Coletto L, Grumati P, Bonaldo P "Misregulation of autophagy and protein degradation systems in myopathies and muscular dystrophies" J Cell Sci. 2013 Dec 1;126(Pt 23):5325-33.
85. Sandri M, Lin J, Handschin C, Yang W, Arany ZP, Lecker SH, Goldberg AL, Spiegelman BM. "PGC-1α protects skeletal muscle from atrophy by suppressing FoxO3 action and atrophy-specific gene transcription" Proc Natl Acad Sci U S A. 2006 Oct 31;103(44):16260-5.
86. Sarbassov DD, Guertin DA, Ali SM, Sabatini DM "Phosphorylation and regulation of Akt/PKB by the rictor-mTOR complex" Science 2005 Feb 18;307(5712):1098-101.

87. Schiaffino S, Mammucari C "Regulation of skeletal muscle growth by the IGF1-Akt/PKB pathway: insights from genetic models" Skelet Muscle. 2011 Jan 24;1(1):4.
88. Schiaffino S, Reggiani C. "Fiber types in mammalian skeletal muscles" Physiol Rev. 2011;91(4):1447-531.
89. Selsby, J., Morris, C., Morris, L. and Sweeney, L. "A proteasome inhibitor fails to attenuate dystrophic pathology in mdx mice" PLoS Curr. 2012; 4, e4f84a944d8930.
90. Sheterline P, Clayton J, Sparrow J "Actin" Protein Profile 1995;2(1):1-103.
91. Shy GM, Engel WK, Somers JE, Wanko T "Nemaline Myopathy. A new congenital myopathy" Brain. 1963 Dec; 86:793-810.
92. Sies, H. Oxidative Stress. Academic press; London: 1985
93. Sparrow JC, Nowak KJ, Durling HJ, Beggs AH, Wallgren-Pettersson C, Romero N, Nonaka I, Laing NG "Muscle disease caused by mutations in the skeletal muscle alpha-actin gene (ACTA1)" Neuromuscul Disord. 2003;13(7-8):519-31.
94. Stanfield CL "Fisiologia" Quarta edizione Edises editor 2011 Cap.12 pag.328.
95. Stankovic-Valentin N, Melchior F "Control of SUMO and Ubiquitin by ROS: Signaling and disease implications" F Mol Aspects Med. 2018 Oct;63:3-17.
96. Suzuki K, Ohno H, Oh-ishi S, Kizaki T, Ookawara T, Fukii J, Radak A, Taniguchi N "Superoxide dismutases in exercise and disease". In: Handbook of oxidants and antioxidants in exercise. Sen C, Packer L, Hanninen O editors. Elsevier; Amsterdam: 2000. p. 243-295
97. Sztal TE, Zhao M, Williams C, Oorschot V, Parslow AC, Giousoh A, Yuen M, Hall TE, Costin A, Ramm G, Bird PI, Busch-Nentwich EM, Stemple DL, Currie PD, Cooper ST, Laing NG, Nowak KJ, Bryson-Richardson RJ "Zebrafish models for nemaline myopathy reveal a spectrum of nemaline bodies contributing to reduced muscle function" Acta Neuropathol. 2015 Sep;130(3):389-406.
98. Talmadge RJ, Grossman EJ, Roy RR "Myosin heavy chain composition of adult feline (Felis catus) limb and diaphragm muscles" J Exp Zool. 1996 Aug 15;275(6):413-20.

99. Towbin H, Staehelin T, Gordon J “Electrophoretic transfer of proteins from polyacrylamide gels to nitrocellulose sheets: procedure and some applications” Proc Natl Acad Sci U S A. 1979 Sep;76(9):4350-4.

100. Trewin AJ, Berry BJ, Wojtovich AP “Exercise and Mitochondrial Dynamics: Keeping in Shape with ROS and AM PK” Antioxidants (Basel). 2018 Jan 6;7(1).

101. Ueda K, Serajee F, Huq AM “A Mutation in the ACTA1 gene Manifesting Nemaline Myopathy with Central Nervous System Lesions” J Clin Neurol. 2017 Jul;13(3):300-302.

102. Wallgren-Pettersson C, Sewry CA, Nowak KJ, Laing NG “Nemaline myopathies” Semin Pediatr Neurol. 2011 Dec;18(4):230-8.

103. Wong HS, Dighe PA, Mezera V, Monternier PA, Brand MD “Production of superoxide and hydrogen peroxide from specific mitochondrial sites under different bioenergetics conditions” J Biol Chem. 2017 Oct 13;292(41):16804-16809.

104. Yang L, Yu P, Chen X, Cai T “The de novo missense mutation N117S in skeletal muscle α-actin 1 causes a mild form of congenital nemaline myopathy” Mol Med Rep. 2016 Aug;14(2):1693-6.